Accepted Manuscript

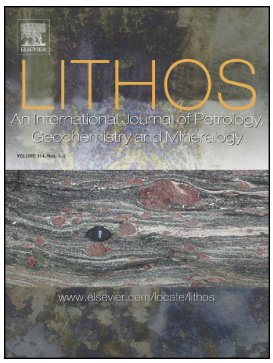

The common origin and alteration history of the hypabyssal and volcanic phases of the Wadi Tarr Albitite complex, southern Sinai, Egypt

Mokhles K. Azer, Hisham A. Gahlan, Paul D. Asimow, Khaled M. Al-Kahtany

PII: S0024-4937(18)30477-8
DOI: https://doi.org/10.1016/j.lithos.2018.12.015
Reference: LITHOS 4906

To appear in: *LITHOS*

Received date: 5 August 2018
Accepted date: 14 December 2018

Please cite this article as: Mokhles K. Azer, Hisham A. Gahlan, Paul D. Asimow, Khaled M. Al-Kahtany , The common origin and alteration history of the hypabyssal and volcanic phases of the Wadi Tarr Albitite complex, southern Sinai, Egypt. Lithos (2018), https://doi.org/10.1016/j.lithos.2018.12.015

The common origin and alteration history of the hypabyssal and volcanic phases of the Wadi Tarr Albitite Complex, southern Sinai, Egypt

Mokhles K. Azer[1], Hisham A. Gahlan[2,3], Paul D. Asimow[4], Khaled M. Al-Kahtany[2]*

[1]*Geological Sciences Department, National Research Centre, Cairo, Egypt*

[2]*Department of Geology and Geophysics, King Saud University, Riyadh 11451, Saudi Arabia*

[3]*Geology Department, Assiut University, Assiut 71516, Egypt*

[4]*Division of Geological & Planetary Sciences, California Institute of Technology, Pasadena CA 91125, USA*

Abstract

New data and interpretations are presented for the igneous albitites of the Wadi Tarr area, southern Sinai, Egypt. The albitite masses are isolated in outcrop from any granitic intrusions and have intrusive contacts against the country rocks without any structural control. They have marginal zones of breccias with jigsaw-fit angular clasts suggesting explosive, in-situ formation. The albitites are of two types: the western, medium-grained, hypabyssal albitite and the eastern, fine-grained porphyritic albitite. The field relations suggest emplacement at different levels in a magmatic cupola: the hypabyssal texture and steeply dipping slope of the upper contact of the western albitite imply deeper emplacement whereas the gently dipping contacts and porphyritic texture of the eastern albitite masses indicate that they define the probable location of the cupola apex. Both types of albitites consist of albite (92-97 %) with minor amounts of quartz, K-feldspar and biotite. The accessory minerals include Fe-oxides, augite, sulphides, zircon, rutile, xenotime, titanite, allanite and monazite. The whole-rock compositions of the hypabyssal and porphyritic albitites are closely related, but the porphyritic type has lower abundances of Sr, Ba, Y, Nb, Th and Zr. We show that the hypabyssal and porphyritic albitites have a common petrogenetic origin, most likely as late-stage cumulates from a fractionating, strongly alkaline A-type magma,

* **Corresponding author:** Prof. Mokhles K. Azer (mokhles72@yahoo.com)

consistent with the compositions of the mafic minerals. The source magma was probably a tephritic liquid; we use MELTS models to show that only a sufficiently alkaline magma follows a differentiation path that both avoids quartz saturation and encounters the alkali feldspar solvus, reaching a residual liquid in equilibrium with highly sodic feldspar. Although the MELTS results show a chemically consistent means of forming igneous albitite, they are incomplete in that physical segregation mechanisms are still required to isolate the albite from mafic minerals and or a low-temperature aqueous alteration stage is needed to leach K from the feldspar. Alteration surrounding the Wadi Tarr albitites is extensive and dominated by alkali metasomatism similar to fenitization. Alteration in the marginal breccia zone of the albitite is dominated by precipitation of amphibole and carbonate in veins and in the breccia matrix, whereas the volcanic country rocks show replacement of feldspars by sericite, carbonate and epidote as well as vein carbonate. The altered volcanic country rocks show lower concentrations of Fe_2O_3, Sr, Cu, Pb, Ba and Ce, accompanied by higher concentrations of Na_2O and MgO compared to unaltered equivalent samples.

Keywords*:* albitite, fenitization, sodic amphibole, cupola, intrusive carbonate, Sinai, Arabian-Nubian Shield

1. Introduction

The rare hypabyssal and volcanic albitite deposits in the Wadi Tarr area of the southern Sinai Peninsula are mined as an albite source. The Tarr albitite complex is one of the youngest intrusive phases (~ 605 Ma; Azer et al., 2010) in the northern tip of the Arabian-Nubian Shield (ANS). It is a igneous albitite with no connection in outcrop to any normal granitoid pluton and is situated in the midst of a volcano–plutonic complex that may be a caldera remnant (Azer et al., 2010; Boskabadi et al., 2013). Crystallization of the Tarr albitites drove expulsion of multiple

pulses of alkali-rich solutions that altered the margins of the albitites and surrounding country rocks, forming fenites (Shimron, 1975; Azer et al. 2010). Excellent exposure of fresh and altered intrusive and extrusive albitites and country rocks in the Tarr area provides a good opportunity to study the petrogenetic processes leading to formation of igneous albitite and associated alteration zones, both of which are of economic interest.

While several previous studies have focused on the intrusive carbonate-albitite of Wadi Tarr (Bogoch et al., 1986, 1987; Azer et al., 2010; Boskabai et al., 2013), the associated alteration zones have received less attention. Several different types of alteration of the country rocks of the albitite have been reported, but a systematic investigation has yet to be carried out. Also, the origin of Tarr albitites is still a matter of debate. A range of mechanisms have been proposed for forming the albitites, from purely metasomatic processes (Bogoch et al. 1987; El-Shazly and Hassanen, 1989) to derivation from mantle-derived magmas (Shimron, 1975, Soliman et al., 1992; Blasy et al. 2001; Azer et al., 2010; Boskabai et al., 2013). Ghabrial et al. (2013) distinguished the Tarr albitites into three subgroups of different origins, specifically rejecting a common origin for the whole deposit. However, in the absence of detailed field work, it is possible that previous authors mistakenly grouped albitite breccia and albitized country rocks (Bogoch et al. 1987; Ghabrial et al., 2013) with the fresh albitite, leading to misinterpretation of the suite.

The present work reports new field studies, petrography, mineralogy and geochemistry of Tarr albitites and volcanic host rocks in the vicinity to determine the albitite sources and to investigate the different alteration zones and their genetic association with albitites. Systematic investigation of the aureole shows that the alteration zone around the Tarr albitite mostly represents classic fenitization rather than the carbonate alteration described by Boskabadi et al. (2013). Our observations and models are synthesized into a simplified tectono-magmatic model for the evolution of the albitites in a magmatic cupola above an alkaline pluton.

2. Geologic Background

2.1. Regional geology

The Neoproterozoic basement rocks of Sinai lie at the extreme northern end of the ANS. They consist essentially of remnants of older metamorphic complexes separated from each other by large volumes of syn-orogenic to post-collisional, mostly unmetamorphosed, granitoid intrusions (Fig. 1a). The Neoproterozoic metamorphic complexes in Sinai are grouped mainly into five outcrops — the Feiran-Solaf, Sa'al-Zaghra, Watir, Kid and Taba metamorphic complexes (Fig. 1a) — although many smaller outcrops of metamorphic rocks are scattered throughout the Sinai massif. The Tarr albitites, the target of the present work, occur within the Kid metamorphic complex (KMC). Detailed studies of the KMC by many authors (e.g. Shimron, 1980, 1984; El-Gaby et al., 1991; Blasband et al. 1997, 2000; Moghazi et al., 2012; Brooijmans et al., 2003; El-Bialy, 2010; Eyal, et al., 2014a) provide background and context.

The KMC represents a volcano-sedimentary succession that underwent several deformation phases and low-pressure metamorphism followed by late to post-orogenic intrusions. Metavolcanic rocks in the Wadi Kid area include rhyolite, rhyodacite, dacite, andesite, and trachyandesite, as well as ignimbrite and other pyroclastic equivalents. The volcanic protoliths have been assigned by some authors to an oceanic island arc setting (e.g. Shimron, 1980; Furnes et al. 1985; El-Metwally 1999; Eyal et al., 2014a) but other authors correlate the volcano-sedimentary successions of Wadi Kid with the subaerial calc-alkaline Dokhan volcanics of the Eastern Desert of Egypt (e.g. El-Gaby et al. 1991; El-Bialy, 2010; Khalifa et al., 2011 and many others). The Wadi Kid metasediments contain sequences of well-bedded pelitic schists, mica-rich phyllites, conglomerates, graywackes and carbonates (Shimron, 1975; Shimron, 1980; Hafez et al. 2007; El-Bialy, 2013). The metamorphic grade of the KMC ranges from greenschist to amphibolite facies (Reymer, 1983; Furnes et al., 1985; El-Gaby et al., 1991; Brooijmans et al., 2003; Eliwa et al., 2008).

Post-metamorphic plutonic rocks in the Wadi Kid area include a gabbro-diorite complex and various granitoid bodies (e.g. Shimron 1980; Moghazi et al. 1998; Shahien, 2002; Azer et al. 2010, 2016). In particular, three plutons in the vicinity of the Tarr area (the Sama quartz monzonite, Lathi monzogranite and Mandar syenogranite) are classified as A-type, late to post-orogenic intrusions with ages ranging from 579 ± 9 to 612 ± 15 Ma (e.g. Be'eri-Shlevin et al. 2009, Ali et al. 2009). A recent U–Pb zircon date of 605 ± 15 Ma for the Tarr albitite (Azer et al. 2010) is synchronous, within error, with the ages of the A-type plutons in the immediate vicinity and with a number of other dated alkaline magmatic suites in the Eastern Desert and Sinai (e.g. Katzir et al. 2007; Moussa et al. 2008; Ali et al., 2009; Be'eri-Shlevin et al., 2009; Ali, 2015, Litvinovsky et al., 2015).

2.2. Local Geology

The Wadi Tarr area occupies the southernmost part of the KMC, along the eastern edge of the southern Sinai (Fig. 1a). The geologic map is dominated by the metamorphosed volcano-sedimentary succession of the KMC. The center of the study area features late Neoproterozoic albitite; outcrops of the syenogranite of similar age are restricted to the eastern edge of the map with no outcrop connection to the albitites (Fig. 1b) (Azer et al., 2010; Boskabadi et al, 2013). The mapped area is characterized by low to moderate relief terrain dissected by numerous structurally controlled wadis, but the Tarr albitites form conspicuous light-colored peaks. The albitite masses are distinguished in the field and in Google Earth satellite images as light-colored areas that stand out from the country rocks and form domal structures (Fig. 2a). The whole area of Wadi Tarr is cross-cut by swarms of mafic and felsic dykes trending in NE-SW direction. Some white-to-pink rhyolitic dykes that cut the KMC country rocks are observed to be truncated against the eastern porphyritic albitite and are highly altered at the contact with the albitite.

For the present study, we collected detailed field observations, concentrating on the contacts between the albitites and their country rocks. The igneous albitites of the Tarr area include the western hypabyssal albitite (exposed in Wadi Tarr itself) and the eastern porphyritic albitite (found in Wadi Ghorabi El-Hatimiya and Wadi Khashm El-Fakh). The main albitite body in Wadi Tarr is an irregular intrusion (<1.2 km^2 in outcrop area), elongated from NW to SE (Fig. 1b). The contacts between albitites and country rocks are sharp intrusive contacts (Fig. 2b) with no evidence of structural control. In most places the margins of the intrusion are marked by altered breccias. Alteration extends typically ~300-500 m into the country rocks; the degree of alteration is locally variable but generally decreases away from the albitite masses. The albitite masses are all devoid of xenoliths and feature many diffuse veins and offshoots of intrusive albitite cross-cutting the country rocks (Fig. 2c). Although such observations imply intrusion of a fluid or melt phase to open the space now occupied by the albite, they should not be taken as evidence that the intruding phase was of pure albite composition (see below). Scattered dark-green dolerite or lamprophyre dykes occur near the albitite margin, dominantly within or close to the breccia zone.

The main albitite mass of Wadi Tarr is medium-grained, with equigranular to inequigranular textures characteristic of hypabyssal emplacement. On the other hand, the small albitite masses of Wadi Ghorabi El-Hatimiya and Wadi Khashm El-Fakh have a porphyritic texture defined by a fine-grained matrix carrying large albite phenocrysts with structural rotation, a distinctively volcanic texture. We carefully documented the attitudes of the exposed contacts. The contacts of the hypabyssal albitite at Wadi Tarr against the country rocks are steeply dipping (60-70^o) (Fig. 2d), whereas the contacts of porphyritic albitite at Wadi Ghorabi El-Hatimiya and Wadi Khashm El-Fakh are relatively flat (25–30°) (Fig. 2e). Also, many small and isolated offshoots of porphyritic albitite permeate the country rocks (Fig. 2f) and extend up to 200 m outside the main porphyritic albitite masses. These observations suggest that the subsurface area

and volume of the albitite intrusion or of associated deeper phases of the magmatic body are considerably larger than the exposed outcrop mass.

Fenite zones ranging in thickness from a few centimeters up to 30 cm are observed at selected outcrops of the hypabyssal albitite margin (Fig. 2g). On the other hand, breccia zones ranging in thickness from a few meters up to 50 m are common around the porphyritic albitite. Well-exposed breccia zones can be subdivided into albitite breccia and volcanic breccia with sharp contacts between the types (Fig. 2h). The albitite breccia (interior to the intrusions) consists of angular albitite clasts in a matrix of dark green fibrous amphibole and minor intrusive carbonates (Fig. 2i). The volcanic breccia (exterior to the intrusions) consists of angular fragments of country rocks, mainly trachytic ignimbrite tuff, cemented by intrusive carbonate. Bogoch et al. (1987) considered the breccia zones around the albitites to be tectonic breccias representing shear zones. We find, however, that the clasts in the breccias display clear angular jigsaw-fit textures suggesting explosive, in-situ formation. They are strictly confined to the margins of the albitites and we find no evidence of structural control.

Veins and dykes (several centimeters up to 30 cm wide) of intrusive carbonate (Fig. 2j) occur in breccia zones proximal to the margin of the albitite bodies and locally extend away into unbrecciated country rocks. Shimron (1975) and Azer et al. (2010) suggested the term carbonatite for such intrusive carbonates in the sense of Heinrich (1966), “carbonate-rich rocks of apparent magmatic derivation or descent”. These are coarsely crystalline and have locally been altered, recrystallized and overprinted by late secondary calcite and breunnerite precipitation in fractures.

3. Analytical methods

A total of 83 thin sections of the albitites and their country rocks were prepared. Based on petrographic examination, thirteen albitite samples (7 hypabyssal albitite and 6 porphyritic albitite) showing no evidence of hydrothermal alteration were selected for whole-rock

geochemical analysis. The breccias were not analyzed because they are universally altered and heterogeneous at hand-sample scale . Twelve volcanic samples (5 altered flows, 5 unaltered flows and 2 rhyolitic dykes) surrounding the Tarr albitites were analyzed for major and trace elements in order to examine the mobility of elements during alteration. Concentrations of major and trace elements were determined by X-ray fluorescence (ThermoARL XRF Spectrometer) at the GeoAnalytical Lab, Washington State University, USA. The powdered samples were weighed, mixed with di-lithium tetraborate flux (2:1 flux:rock), fused at 1000 °C in a muffle furnace, and cooled; the resulting bead was reground, refused and polished on diamond laps to provide a smooth, flat analysis surface. Reference material 650CC from GSP2 was used as calibration standard. The analytical precision for XRF analyses, as calculated from duplicate samples, is better than 1% for most major elements and better than 5% for most trace elements (except Ni, Cr, and V); standard accuracy and reproducibility data and detection limits are documented in Johnson et al. (1999). Loss on ignition (LOI) is determined by weight difference after firing at 1000 °C.

Rare-earth element (REE) and selected trace element concentrations of 14 samples (8 albitite and 6 volcanic) were analyzed at ACME Analytical Laboratories, Canada, by inductively-coupled plasma mass spectrometry (ICP-MS), following a lithium metaborate/tetraborate fusion and nitric acid digestion of a 0.2 g sample. Duplicate measurements provided a precision generally better than 2% (SD) except for Er and Lu (<4%). The accuracy of the analyses was monitored by a series of international reference materials. The analytical precision and detection limits for ACME analyses are listed on the laboratory website (http://acmelab.com/services/method-descriptions).

Electron microprobe analyses of the essential, accessory and secondary minerals from the albitites and volcanics were performed in polished sections using a five-spectrometer JEOL JXA-8200 electron microprobe at the Division of Geological and Planetary Sciences (GPS), California

Institute of Technology, USA. Operating conditions were 15 kV accelerating voltage, 25 nA beam current, a focused beam (1 μm), 20 second on-peak counting times, a mix of natural and synthetic mineral standards, and the CITZAF matrix correction routine. Amelia albite, the Na standard, experiences beam damage at a rate similar to the unknown albites; use of the nominal composition of albite standard therefore recovers, to acceptable accuracy, stoichiometric feldspar compositions with fully occupied A sites.

4. Petrography

Detailed petrographic descriptions of the albitites, breccias and country rocks are given in the following sections.

4.1. Albitites

According to the IUGS (1989), albitite is a variety of alkali feldspar syenite consisting almost entirely of albite. Petrographic examination confirms a clear distinction between the two types, i.e. the western hypabyssal albitite of Wadi Tarr and the eastern porphyritic albitite of Wadi Ghorabi El-Hatimiya and Wadi Khashm El-Fakh. Both albitites are very fresh and non-metamorphosed, confirming the field and geochronological inference that albitite formation postdates the Kid regional metamorphic event. The modal abundance of albite is 92- 97%.

The porphyritic albitite is fine-grained with a variable fraction of albite phenocrysts (5-20 vol. %) set in a microcrystalline felsic groundmass. Fe-oxides, sulphides, zircon, rutile, monazite and xenotime are accessory minerals. The phenocrysts occur either as discrete crystals or as glomerophyric clusters. Phenocrysts are mostly prismatic in shape and may reach 4.0 mm in length and 2.0 mm in width. They usually show simple twinning and/or albite-Carlsbad twinning (Fig. 3a, b). We observe rare microphenocrysts of clinopyroxene (<0.3 mm), not previously reported in the Tarr albitite, as anhedral cracked crystals altered along the margins into secondary

amphiboles (Fig. 3c). The groundmass is felsic in composition and shows various textures, including granular and micrographic textures. Minor muscovite and carbonates are observed only in the porphyritic albitite variety.

The hypabyssal albitite is leucocratic and pale yellow to white or grey in colour. It shows typically medium-grained granitoid textures, consisting essentially of randomly oriented euhedral to subhedral albite crystals (95-97%) as the major constituent with very minor quartz (<4%), orthoclase (1-4%) and biotite (<1%). Accessory minerals include zircon, titanite, allanite, rutile, monazite and xenotime. Secondary minerals include sericite, chlorite and Fe-Ti oxides. Albite grain size in some samples is quite homogeneous, whereas other thin sections exhibit a substantial range of albite crystal sizes. Crystals are all twinned on the albite law; twin lamellae are usually narrow and numerous. Carlsbad twinning is comparatively rare. The crystals are usually fresh, though slight turbidity may sometimes occur along the cleavage cracks. No evidence of zoning was seen. Quartz occurs as small crystals or is completely absent. Orthoclase occurs in small amounts, forming small crystals of irregular shape up to 0.5 mm across. Rare anhedral interstitial biotite crystals (<0.25 mm) with altered margins are observed among the albite (Fig. 3d). Chlorite occurs as green spots formed by the decomposition of a ferromagnesian mineral, probably after aggregates of biotite flakes.

4.2. Fenite margins

Samples were collected from the fenite margins around the hypabyssal albitite. These margins consist essentially of fine to medium-grained albite and carbonate. Albite occurs as anhedral to subhedral, poorly twinned and 'checkerboard'-textured albite that appears to have locally replaced polysnthetically twinned albite. Carbonates (up to 20-30 vol.%) exhibiting ubiquitous stress twinning occur interstitially.

4.3. Breccias

Two types of breccia are distinguished, namely interior albitite breccias and exterior volcanic breccias (Azer et al., 2010; Boskabadi et al, 2013). Both types contain less than 25 percent matrix and are mostly clast-supported.

The albitite breccia is comprised of angular fragments of albitite in a matrix of fibrous secondary amphiboles, albite and carbonates with trace accessory allanite and xenotime. Most of the albitite rock fragments are medium-grained albitite variably and pervasively replaced by sericite and carbonate and commonly traversed by microfractures. The albite in the matrix is fine-grained and fresh and is seen to cross-cut the coarser first-generation albite crystals. Quartz occurs in the matrix of the albitite breccia zone as strained anhedral crystals showing undulatory extinction or as vug fillings. Primary biotite has been completely altered to chlorite and iron oxides. Secondary amphiboles occur as coarsely crystalline actinolite (Fig. 3e) or locally as fibrous interfragmental cement (Fig. 3f). Carbonates include dolomite and calcite, found as large fragments, cements and fracture-fillings associated with actinolite and chlorite. Very rare aggregates of sodic amphiboles are observed within the albitite breccia (Fig. 3g). Locally, the albitite breccia contains clusters of secondary minerals (apatite + fluorapatite + allanite ± monazite ± xenotime ± rutile ± zircon) in the carbonate groundmass.

The volcanic breccia consists of angular to sub-angular rock fragments of andesitic to trachyandesitic tuff; the rock fragments are highly sericitized (Fig. 3h) due to K-metasomatism. Carbonate alteration is more abundant in the volcanic breccia than in the albitite breccia. Carbonates form veins and fracture fillings. Breunnerite is more common than dolomite and is often associated with rutile, apatite and secondary iron oxides. Secondary albite, muscovite, and phlogopite are common in the volcanic breccia zone. Fibrous actinolite is present in the matrix but rare. Epidote, mostly anhedral red or reddish brown piempontite, usually occurs as vug fillings (Fig. 3i) or replacing pre-existing plagioclase and ferromagnesian minerals.

In both kinds of breccia samples, carbonates occur as cements, veins and dyke-like bodies. Dolomite and breunnerite are common; calcite is rare. The dolomite is white to light grey, forms mostly coarse to medium-grained aggregates, and shows perfect rhombohedral cleavages and sometimes pressure twining. Accessory minerals associated with intrusive dolomite are apatite, chlorite and iron oxides. The breunnerite is dark brown in color with dark iron-manganese oxides along cleavage planes and rhombic boundaries. Breunnerite typically appears cross-cutting dolomite with sharp contacts. Accessory minerals associated with breunnerite are rutile, sericite, chlorite, pyrite and secondary Fe-Mg oxides.

4.4. Country rocks

Beyond the exterior volcanic breccia zone, volcanic and metasedimentary country rocks are exposed with degrees of alteration decreasing away from the albitite bodies. Both altered and unaltered volcanic country rocks were collected to represent the outer alteration zone for this study, including ignimbrite, crystal tuff, and banded tuff of trachyandesite to andesitic composition. The main phenocrysts and crystal fragments in crystal tuffs are plagioclase and quartz with minor K-feldspar, biotite, chlorite, sericite and epidote. Banded tuffs are very fine-grained and composed of alternating laminae of vitreous-ashy material of variable colours. The ignimbrites contain flattened lenticular glass particles (fiamme) with a well-defined preferred orientation, embedded in a groundmass. The groundmass includes crystals and crystal fragments of plagioclase and quartz. The groundmass in most of the ignimbrite samples examined is devitrified into equigranular crystal aggregates showing mosaic texture, and rarely shows a fluidal structure.

The alteration degree of the country rocks is locally variable, but generally decreases away from the contact with the exterior breccia zone. Alteration of the volcanic rocks manifests at thin section scale as increased modal abundances of sericite, chlorite and muscovite as well as

appearance of secondary carbonate. The concentration of alteration activity along fractures is evident at multiple scales. Plagioclase crystal fragments in the crystal tuffs are pervasively replaced by sericite and muscovite (Fig. 3j). Secondary albite is observed in the altered volcanic rocks as discrete fine-grained crystals and as patches of albite associated with platy muscovite (Fig. 3k). Secondary albite also occurs as overgrowths around primary albite (Fig. 3l) and as veinlets cross-cutting the groundmass. Localized stellate chlorite aggregates have also replaced the albite-carbonate host assemblage.

Metasedimentary country rocks are common around the eastern porphyritic albitite, and appear as small exposures intercalated with the volcanic country rocks at the western albitite. They are represented by schists that have been locally mylonitized but not obviously affected by the albitite alteration halo. Schists contain cordierite in a groundmass of biotite, chlorite, sericite and opaque minerals. Previous studies have shown that the metamorphic grade of the volcano-sedimentary successions in the Tarr area is mostly greenschist facies (Shimron, 1975, 1984; Reymer, 1983; Soliman et al., 1992), which is consistent with the petrography of the schists. However, the present field and microscopic investigations indicates that the volcanic rocks in the vicinity of the Tarr albitite are unmetamorphosed except for the alteration around the albitite.

5. Mineral chemistry

The essential minerals (feldspars) and some accessory minerals (biotite, pyroxene, and zircon) were analyzed in hypabyssal and porphyritic albitite samples. Also, some secondary minerals including biotite and amphiboles were analyzed in unaltered volcanic country rock samples. All electron microprobe data are given in the Supplementary Tables (1S-7S).

5.1. Pyroxene

Rare fine crystals of pyroxene were analyzed from the porphyritic albitite and their chemical compositions and structural formula are given in Supplementary Table 1S. They are fairly restricted in their compositional range, with high CaO (16.3-18.7 wt.%), MgO (10.8-13.7 wt.%) and FeO (12.9-15.7 wt.%) contents, and low concentration of low Al_2O_3 (<0.9 wt.%), TiO_2 (<0.5 wt.%), K_2O (<0.02 wt.%) and Na_2O (<0.5 wt.%). They are classified as augite according to Morimoto et al. (1988) (Fig. 4a). Mg# [(Mg/(Mg+Fe^{+2})] of the analyzed clinopyroxene ranges between 0.56 and 0.65 with an average of 0.59. These pyroxene compositions are similar to those described in late Ediacaran post-collisional A-type syenites throughout south Sinai (e.g. Eyal et al., 2014b; Moreno et al., 2014; Azer et al., 2015; Gahlan et al. 2016).

Pyroxene is widespread in magmatic rocks and plays an important role in igneous petrogenetic studies (Le Bas, 1962; Nisbet and Pearce, 1977; Leterrier et al., 1982; Lindsley, 1983; Rietmeijer, 1983; Akinin et al., 2005). According to the Lindsley (1983) calibration, clinopyroxene in the porphyritic albitite indicates crystallization temperatures from 900 to 1100 °C (Fig. 4a). The Mg# and crystallization temperatures both suggest that the rare augite found in the porphyritic albitite is an early-crystallized mineral, inherited from the magma chamber before emplacement. The estimated temperature is comparable to temperature inferences that have been published for the parental magmas of post-collisional syenitic rocks in south Sinai (Eyal et al., 2014b; Moreno et al., 2014; Azer et al., 2015; Gahlan et al., 2016).

5.2. Biotite

Sparse fresh relics of biotite in the hypabyssal albitite and secondary biotite in the altered volcanic country rocks were analyzed. The chemical compositions and structural formula of the analyzed biotite are given in Supplementary Table 2S. The primary biotite is richer in SiO_2, TiO_2, Cr_2O_3, MnO, MgO and K_2O, but lower in FeO and CaO than the secondary biotite. The secondary biotite has very high FeO*/MgO ratios (10.2-23.0) and is classified as annite. Biotite from the

hypabyssal albitite samples shows typical chemical characteristics of primary igneous biotite, whereas the biotite in altered volcanic country rocks extends into the field of typical secondary biotite (Fig. 4b) (Nachit et al., 2005).

The sparse fresh relics of primary biotite in the hypabyssal albitite have FeO*/MgO (1.9-2.7) ratios typical of alkaline biotite (Abdel-Rahman 1994), which is confirmed by plotting the biotite analyses on the Al_2O_3-FeOt discrimination diagram (Fig. 4c). On the same diagram, the biotite analyses are similar to biotite from post-collisional syenitic rocks throughout south Sinai (e.g. Farahat and Azer, 2011; Azer et al., 2014; Eyal et al., 2014b; Moreno et al., 2014; Gahlan et al., 2016).

5.3. Amphiboles

Amphibole analyses are provided from altered volcanic country rocks (Supplementary Table 3S). The analyzed amphiboles have low TiO_2 (<0.1) and contain < 0.01 Ti p.f.u. which characteristic for secondary amphiboles (Girardeau and Mevel, 1982). The very rare sodic amphiboles observed in thin section (Fig. 3g) were not analyzed by electron probe. According to the classification scheme of Leake et al. (1997), all the analyzed amphiboles are calcic, with Ca ranging from 1.7 to 1.9 atoms per formula unit. They include actinolite and actinolitic hornblende with rare magnesio-hornblende (Fig. 4d). On the discrimination diagram proposed by Keeditse et al. (2016), the analyzed amphiboles plot in the field of secondary amphiboles (Fig. 4e).

5.4. Feldspars

Feldspars were analyzed in both hypabyssal and porphyritic albitites; chemical compositions and structural formulae are given in Supplementary Tables 4S, 5S and 6S. The analyzed feldspars are mainly albite with rare crystals of K-feldspars. We were unable to resolve any zoning, indicating crystallization probably close to equilibrium conditions (Azer et al., 2015).

Albite in both albitites variety is nearly pure and similar in composition, having very low An contents (< 3%) with high Ab contents (> 97%). The K-feldspars are nearly pure orthoclase (Or > 95).

5.5. Accessory minerals

The Tarr albitites include a significant variety of accessory minerals, including zircon, Fe-oxides, sulphides, xenotime, titanite, allanite and monazite. Among these, given the list of elements included in the electron probe analytical protocol used, it is only practical to report compositions of zircon. Chemical analyses of zircon together with their structural formulae are given in Supplementary Table 7S. Zircon shows limited variation in composition, with a maximum 2.2 wt. % HfO_2. HfO_2 in zircon from hypabyssal albitite ranges from 1.8 to 2.2 wt.%, while in the porphyritic albitite the zircon HfO_2 abundance is lower (1.3-1.6 wt.%).

6. Geochemistry

6.1. Geochemical characteristics of albitites

Several studies of the geochemistry of the Tarr albitites are available (Blasy et al., 2001; Azer et al., 2010; Boskabadi et al., 2013; Ghabrial et al., 2013) that nominally show large variations in the chemical composition of albitite. We argue that this reflects inclusion of unrelated rock types and altered varieties. Ghabrial et al (2013), for example, report an analysis of equigranular albitite with high silica content (up to 77.95 wt.% SiO_2), which corresponds to at least 30% normative quartz and hence is not an albitite. No such anomalously SiO_2-rich albitite was observed in this study or any other published works (Blasy et al., 2001; Azer et al., 2010; Boskabadi et al., 2013).

The newly reported chemical analyses of the western hypabyssal albitite and eastern porphyritic albitite, are given in Table 1, expressed as oxide weight percents, trace element

concentrations, and normative mineral abundances. In terms of major element compositions, the Tarr albitites are broadly syenitic, as SiO_2 contents range from 66.5 to 69.3 wt%. They are, as expected, high in Al_2O_3 (18.8-20.0 wt%) and Na_2O (10.0-11.1wt%), reflecting the high contents of modal and normative albite. They have low contents of TiO_2 (0.3-0.4 wt.%), MgO (0.0-0.5 wt.%), $Fe_2O_3^T$ (0.3-0.5 wt.%), K_2O (0.1-0.3 wt.%) and P_2O_5 (0.1-0.3 wt.%). Hypabyssal albitite is very similar to porphyritic albitite, except that hypabyssal albitite has systematically higher abundances of Nb, Sr, Ba, Y and Zr than porphyritic albitite.

The whole-rock compositions of Tarr albitites mainly plot in the syenite field on the R1-R2 classification diagram of De la Roche et al. (1980) (Fig. 5a), as expected from their petrography. CIPW normative compositions indicate that albite is the dominant feldspar (84.4-94.5%) and samples yield a wide range of normative quartz, from 0.2 to 7.9 %. All the analyzed samples have some normative corundum (0.3-2.1 %). The Tarr albitites are metaluminous, with alumina saturation index [ASI = molar ratio $Al_2O_3/(CaO+Na_2O+K_2O)$] ranges between 1.0 and 1.08.

All the albitite samples have agpaitic index [AI = molar (Na+K)/Al] greater than 0.87 (0.88-0.97), which is typical of alkaline rocks (Liégeois and Black, 1987; Liégeois et al., 1998). The field relations and geochemical characteristics of the albitites show broad similarity to A-type granitic rocks of southern Sinai. On the Ga/Al vs. Nb discrimination diagram of Whalen et al. (1987) the albitites (especially the hypabyssal samples) dominantly plot in the field of A-type granite (Fig. 5b).

Normalized trace element plots ("spider diagrams") for the hypabyssal and porphyritic albitites, using the MORB normalization values of Pearce (1983), are shown in Figure 5c. It is clear that the each albitite type forms a homogeneous population and that the two types show strong general similarities in their patterns. They display depletion in K, Sr, Rb, P, Ti and

enrichment in Th. K, Sr and Rb depletions may be due to leaching of alkalis during alteration (see below)..

Results of REE analyses are given in Table 2 and chondrite-normalized REE patterns (using the chondrite values of Evensen et al., 1978) are presented in Figure 5d. Chondrite-normalized REE patterns for the Tarr albitites show LREE enrichment [$(La/Lu)_n$= 4.18-10.50] and almost flat HREE profiles [$(Gd/Lu)_n$=1.44-1.76], typical for the ~600 Ma A-type granitic rocks of the ANS (e.g. Katzir et al., 2007; Azer, 2013; Khalil, 2018). The porphyritic albitite samples have lower REE contents (∑REE= av. 133 ppm) than the hypabyssal albitite samples (∑REE= av. 166 ppm), with the differences in total REE dominantly controlled by the light REE (LREE) abundances. It is likely that this simple reflects differences in the modal abundance of LREE-rich accessory phases. Both albitites have slightly to moderately negative Eu-anomalies [(Eu/Eu*)=0.55-0.76] similar to ~600 Ma A-type ANS granite.

6.2. Geochemical characteristics of surrounding volcanics

The chemical analyses of the altered and unaltered volcanic country rocks and two rhyolitic dykes are shown in Table 3. Of course the country rocks, not being dominated by albite, differ in whole-rock chemistry from the albitites in having higher K_2O, lower Na_2O, and lower Al_2O_3 (15.7-16.8 wt.%). Based on the silica contents (60.0-63.2 wt.% SiO_2) of the volcanic country rocks surrounding albitite bodies, they have basaltic-andesite and andesite compositions (Fig. 6a), while the felsic dykes are rhyolite (73.8-74 wt.% SiO_2). The rhyolitic dykes are much richer in Na_2O (7.4-8.0 wt.%) than K_2O (2.1-2.8 wt.%), which might be attributable to Na-metasomatism associated with intrusion of albitite. Similar rhyolitic dykes near the Tarr albitites were incorrectly grouped with the porphyritic albitite by Ghabrial et al. (2013), leading to misinterpretation of the genesis of the albitites.

The altered volcanic host rocks proximal to the volcanic breccia are enriched in Na_2O, K_2O and MgO and depleted in CaO compared to more distal volcanic samples. This accords with the greater abundance of secondary minerals such as albite, sericite, muscovite, actinolite and chlorite in the more strongly altered samples. Trace element analyses of the altered volcanic rocks adjacent to the volcanic breccia also imply redistribution of some elements. The clearest systematic chemical mobility is observed in Sr, Cu, Pb, Ba and Ce, which are depleted in the altered volcanic samples relative to their unaltered equivalents.

The volcanic country rocks have ASI ranging between 0.89 to 1.12, indicating metaluminous character. They all have AI less than 0.87 (Table 3), characteristic of calc-alkaline rocks (Liégeois and Black, 1987; Liégeois et al., 1998). The unaltered volcanic samples are characterized by enrichment of large ion lithophile elements (LILEs: K_2O, Sr, Rb, Ba, Th) relative to high field strength elements (HFSEs: Nb, Y, Zr, Yb) (Table 3), a typical feature of continental-arc rocks formed through active margin-related processes (Pearce et al., 1984; Grove et al., 2003). The relatively high contents of K_2O (3.6-4.3 wt.%), Ba (453-708 ppm) and Sr (387-564 ppm) as well as the high Zr/Y ratios (8.5-11.0) of the unaltered volcanics are typical of calc-alkaline magmas formed along continental arc margins (Pearce, 1983; Wilson 1989).

The MORB-normalized spider diagrams of the volcanic country rocks are given in Fig. 6b. The spider diagrams of the altered volcanics are similar to those of unaltered varieties, but concentrations of nearly all of the plotted trace elements are systematically lower in the altered volcanics than in the unaltered varieties (most markedly so in Sr and Ba). All the patterns are characterized by enrichment in large-ion lithophile elements (LILE) relative to high field-strength elements (HFSE) with small negative anomalies in Ta-Nb. The negative P and Ti anomalies can be attributed to apatite and Fe-Ti oxide fractionation at earlier stages of magmatic evolution. These patterns are characteristic of the post-collisional volcanic rocks in the Eastern Desert and

Sinai, such as the Dokhan volcanic series (e.g. Be'eri-Shlevin et al., 2011; Azer and Farahat, 2011; Obeid and Azer, 2015; Abdelfadil et al., 2018).

The chondrite-normalized REE patterns of the volcanic country rocks and the rhyolitic dykes (using the chondrite values of Evensen et al., 1978) are presented in Fig. 6c. The REE patterns of the volcanic country rocks show moderate LREE-enrichment [$(La/Lu)_n$= 4.7-7.1] with a break in slope at Nd, and exhibit either weakly negative or negligible Eu anomalies [(Eu/Eu*)=0.8-1.0], while the HREE patterns are nearly flat [$(Gd/Lu)_n$=1.2-1.6]. The altered volcanics have slightly lower LREE than unaltered volcanics, whereas all the volcanic samples overlap in HREE concentrations. The rhyolitic dykes are characterized by lower REE abundances than either the altered or unaltered volcanic country rocks, indicating different origin. They have moderately negative Eu anomalies [(Eu/Eu*) ~ 0.7]. The REE patterns of the rhyolitic dykes are nearly similar to the samples labeled "high silica albitite" by Ghabrial et al. (2013) (Fig. 6d).

7. Discussion

7.1. Alteration surrounding the Tarr albitites

The present studies indicate that the emplacement of the Tarr albitite into its country rocks was characterized by pervasive alteration, conspicuously shown in marginal breccia zones and extending a few hundred meters beyond the albitite masses. Although the exposed outcrop area of the albitite seems perhaps too small to provide either the required heat source or the required fluid volumes to drive alteration of such a large halo, the field evidence cited above suggests a substantially larger subsurface area and volume of intrusion. We cannot construct a quantitative heat or mass balance model from the observations at hand, but nonetheless the genetic link between the Wadi Tarr albitites and their surrounding alteration zones is evident and hence we are confident that sufficient heat and fluid sources were present. The alteration zones surrounding the Tarr albitite have been interpreted as fenite zones with intense sodium and potassium

metasomatism (Shimron, 1975; Azer et al. 2010). Fenites are metasomatic products demonstrating pervasive modification of precursor wall rocks that interacted with emanations from alkaline silicate or carbonatite magmas (e.g. Bates and Jackson, 1987; Zharikov et al., 2007; Le Bas, 2008; Elliott et al., 2018). However, fenitization is rather a generic process; in the current study area there is evidence that the alteration products are variable in character, which may reflect variations in the protoliths or in fluid composition, permeability, structure, temperature and pressure. We find evidence that multiple pulses of fluid penetrated the surrounding country rocks during albitite emplacement, driving at least four penecontemporaneous fenite alteration events that we distinguish as (1) carbonation, (2) amphibolitization, (3) Na-metasomatism and (4) K-metasomatism.

Carbonate alteration is the dominant process in the breccia zones around the Tarr albitites (Azer et al., 2010; Boskabadi et al., 2013). Textural relations between the carbonate and the brecciated blocks indicate that carbonate formation occurred after explosive degassing took place and was mainly focused along a narrow (25-30 m) zone of brecciation encompassing both the marginal zone of the albitite intrusion and the most proximal zone of the volcanic country rock. It is possible that the explosion was driven by exsolution of the same carbonic fluid that subsequently caused the alteration, or these may involve two subsequent fluid formation and migration events. The various lithologies reacted differently to the carbonic hydrothermal fluid. Carbonate alteration in the albitite breccia appears mainly as precipitation of dolomite in veins and throughout the breccia matrix as cement, whereas in the altered volcanic rocks dolomite replaced feldspars and cross-cutting vein carbonates are dominated by breunnerite. The degree of carbonate alteration is variable in the volcanic breccia, with some samples preserving the original volcanic textures and others partially to completely recrystallized.

Na-metasomatism associated with the Tarr albitites manifests in the albitization of feldspar in the external (volcanic country rock-hosted) breccia zones. Rare aggregates of sodic amphibole

are also observed within the breccias zones, which is likely also a product of Na-metasomatism. Albitization is common in the external breccia zones and decreases in intensity with distance from the albitite. Secondary albite occurs in the altered, brecciated volcanic country rocks as discrete crystals, patches, and (locally) in albitite veinlets. Albitization is a subsolidus metasomatic exchange process by which Na-rich fluids interact with Ca-bearing primary plagioclase, resulting in textural and mineralogical changes to the host lithology. The products of Na-metasomatism described here differ from typical fenites, which usually contain sodic pyroxene (aegirine or aegirine-augite) and amphibole (magnesio-arfvedsonite to eckermannite), as described for example in the Cape Verde and Canary Islands (Le Bas 1981). The difference may be explained by the metaluminous/peraluminous syenitic character of the magmatic source for the fluids at Wadi Tarr, as opposed to the peralkaline parental magma in the ocean island cases (Kinnaird and Bowden 1991). Some differences might also be attributed to pressure at the exposed level of emplacement, as sodic metasomatism associated with deeper intrusions tends to progress towards potassic metasomatism at shallower erosional levels (Kinnaird and Bowden 1991). Na-metasomatism and albitization of the volcanic country rocks may be responsible for the description in Ghabrial et al. (2013) of an altered high silica rhyolite (71.4-74 wt% >SiO_2) as metasomatic albitite.

K-metasomatism is represented mainly by development of secondary muscovite and phlogopite in the external breccia zone. In the altered unbrecciated volcanic country rocks, incipient alteration of albite to sericite, formation of accessory platy biotite, and replacement of biotite by chlorite are all associated with fenitization. The low K_2O contents of the preserved albitite may not be a primary magmatic feature. Rather it may reflect nearly complete loss of magmatic potassium into the country rocks during the fenitization process. Potassium added to the altered country rocks was likely transported from the albitite into the alteration zone by late magmatic fluids expelled from the intrusion. Since the hydrothermal circulation was an open

system, it is possible that K-bearing fluids escaped, so attempt to mass balance the potassium budget of the intrusion and the country rocks are likely to be uninformative.

Amphibolitization occurred throughout the internal and external brecciation zones, where secondary amphiboles occur as coarsely crystalline actinolite or locally as fibrous interfragmental cement.

In order to discern the chemical variations that occurred during alteration of volcanic country rocks, the altered and unaltered volcanic rocks are plotted on a series of diagrams shown in Figure 7. Despite some chemical variability in both the altered and unaltered sample populations, the two populations are clearly distinct and non-overlapping, which makes is possible to plainly recognize the chemical effects of alteration with the collected sample suite. The altered volcanic rocks have lower concentrations of Fe_2O_3, Sr, Cu, Pb, Ba and Ce compared to their unaltered compositions. In contrast, Na_2O and MgO concentrations are higher in the altered samples compared to the fresh samples. These chemical changes are consistent with the greater abundance of secondary minerals (albite, sericite, muscovite, actinolite, chlorite, dolomite, and breunnerite) in the altered volcanics. Hydrothermal alteration of K-feldspar and plagioclase to sericite + carbonate ± epidote leads to leaching of Fe_2O_3, K_2O, and fluid-mobile trace elements. Enrichment of CaO and MgO in the altered volcanic samples is attributed to precipitation of disseminated and vein carbonates.

7.2. Genesis of the Tarr albitite

Albitites occur in a wide variety of geological environments and apparently can be formed by both igneous and metasomatic processes (e.g. Pin, 2006; Mark, 2007; Azer, 2010; Boskabadi et al., 2013). The origin of the Tarr albitites in particular has been a matter of significant debate, with some authors favoring a metasomatic model (Bogoch et al. 1987; El-Shazly and Hassanen, 1989) and others preferring fractional crystallization from or liquid immiscibility in a mantle-

derived magma (Shimron, 1975, Soliman et al., 1992; Blasy et al. 2001; Azer et al., 2010). Some of the confusion may result from differing classification of the rocks in the area; for example, some authors misleadingly group the albitite breccia with the primary albitite. Ghabrial et al. (2013) distinguished the Tarr albitites into three subgroups and assigned each group a different origin. The classification of Ghabrial et al (2013) was based on the statistical treatment of geochemical analyses of unrelated rock types including albitites, breccias and high-silica altered volcanic rocks. However, a high-silica (> 74-80 wt.% SiO_2), low-alumina (<12 wt. % Al_2O_3) altered volcanic rock is simply not an albitite. Albitite, by definition, should be >95% modal albite and hence can contain *at most* 70.3 wt. % SiO_2. Only four samples (WH1, UB1, WF3 and WT2) among the 11 samples described by Ghabrial et al. (2013) are albitite; the remaining analyses represent altered rocks including breccias and volcanic country rock. Sample WF3 in Ghabrial et al. (2013) was labeled carbonate-bearing albitite, despite very low CaO (0.61 wt.%), MgO (0.03 wt.%) and LOI (0.75 wt.%) and high total (~102 wt. %). Also, Ghabrial et al. (2013) based their interpretation of two different origins for the albitite suite on the presence in their sample suite of two distinct groups of REE patterns. Yet, none of their REE analyses are from the typical albitite samples; they are all altered porphyritic volcanics with rhyolitic composition (WF2, WH3 and UB2; 71.4-74 wt.% SiO_2). In fact, as we show in this work, there is only one population of REE patterns in all the fresh albitites, whether hypabyssal or porphyritic. In agreement, then, with every other author that has studied the Tarr albitites — both those that prefer an igneous origin and those that prefer a metasomatic origin! — we see no evidence for multiple unrelated origins for the actual albitite members of the suite.

Recent isotopic investigations of the albitites by Azer et al. (2010) yield restricted ranges of initial $^{87}Sr/^{86}Sr$ (0.7035-0.7038) and $\varepsilon Nd_{605\ Ma}$ (+4.3 to +6.4) and indicate a mantle origin. The similarity in isotopic composition of the albitite and associated intrusive carbonates (dolomite) strongly support a petrogenic link between these rocks (Bogoch et al., 1986; Azer et al. 2010).

However, the isotopic composition of the cross-cutting vein breunnerite (mean $\delta^{18}O$ = +18.85 ‰; mean $\delta^{13}C$ = -6.1 ‰; mean εNd = +2.2; mean $^{87}Sr/^{86}Sr$ = 0.70805) suggests at least partial re-equilibration of the fluid from which the breunnerite precipitated with a sedimentary carbonate source (Azer et al. 2010). The Nd–Sr isotope composition of the Tarr albitites (Azer et al., 2010) is similar to that of other ~600 Ma igneous rocks from the region (Beyth et al. 1994; Katzir et al. 2007). Furthermore, the U–Pb zircon age of 605 ± 15 Ma (Azer et al. 2010) for the Tarr albitite is synchronous, within mutual uncertainty, with the ages of three other plutons in the immediate vicinity (Lathi monzogranite, Sama quartz monzonite and Mandar granite; Be'eri-Shlevin et al. 2009), and of other alkaline magmatism in the Eastern Desert and Sinai (Katzir et al. 2007; Moussa et al. 2008; Eyal et al. 2010; Azer et al. 2010; Farahat and Azer, 2011).

The present work — on the basis of field investigations, petrography, mineral chemistry, and whole-rock compositions — implies a magmatic origin for the Tarr albitites, in agreement with most other published work (Shimron, 1975, Soliman et al., 1992; Blasy et al. 2001; Azer et al., 2010). However, among magmatic models there remain a variety of proposed scenarios and parental magmas, including: (1) fractional crystallization of a gabbroic magma (Shimron, 1975; Blasy et al., 2001), (2) fractional crystallization of a monzonitic magma (Bentor and Eyal, 1987), (3) fractional crystallization of a syenitic magma (Soliman et al., 1992), and (4) residual magma remaining after near-total crystallization of an A-type granite pluton at depth (Azer et al., 2010). In principle, liquid immiscibility offers yet another class of magmatic origin hypotheses, but no experimental or computational evidence suggests that nearly pure albite liquid lies in the vicinity of any miscibility gap.

The P and Ti troughs in the MORB-normalized spider diagram (Fig. 6b) likely reflect the fractional crystallization of apatite and Fe-Ti oxides from the parental magma at a stage earlier than the accumulation of the albitites. The negative Eu-anomalies [(Eu/Eu*)=0.55-0.76] of the

albitites are interpreted to indicate early fractionation of Ca-bearing plagioclase from the parental magma, again at an earlier stage than the development of the albitite.

Formation of igneous albitite is a challenge to igneous petrologists because most common magmatic liquid lines of descent converge on petrogeny's residua system, i.e. the wet granite minimum, which features quartz-saturated magmas and orthoclase-rich feldspars. In fact, even moderately alkaline magmatic suites with monzonitic primitive members generate liquid lines of descent that turn towards the granite minimum, becoming quartz-saturated at high degrees of differentiation (Bucholz et al. 2014a, b) and terminating in aplite rather than albitite. Hence it is necessary to find a magmatic evolution that is both sufficiently alkaline to avoid becoming enriched in quartz by fractionation of feldspars and at the same time sufficiently high in Na/K ratio to avoid becoming enriched in orthoclase. Furthermore, the development of a liquid composition that is sufficiently close to albite stoichiometry to crystallize as a pure albitite is phenomenally unlikely; it requires a perfect balance of initial ASI and AI, because crystallization of feldspars represents a thermal divide that will drive residual liquids either up or down in $Al_2O_3/(Na_2O+K_2O)$ and $Al_2O_3/(CaO+Na_2O+K_2O)$ relative to feldspar stoichiometry. Hence, models that can produce abundant cumulate albite and allow escape of a (not necessarily albite-composition) low-viscosity, hydrous residual liquid seem enormously more probable than models requiring albitic liquid. Such models must occur in the cupola of a nearly crystallized magma chamber with upwards escape or eruption of the residual liquid because — unlike development of monomineralic anorthosite by crystal flotation from gabbroic magma — albite is negatively buoyant in silicic, peralkaline, hydrous residual liquids. These arguments remain true even in light of the field observation of crenulated, intrusive contacts between pure albite and country rocks; although the space now filled by the albitite within the country rock was likely opened by intrusion of a melt or fluid phase, this does not imply that the intruding phase had the same composition as the final rock eventually preserved adjacent to the contact.

We investigated magmatic evolutions that might lead to albitite using a series of forward models of fractionation of primitive A-type magmas using the rhyoliteMELTS 1.1 calibration, an update to the thermodynamic MELTS model (Ghiorso and Sack 1995) that correctly locates the quartz saturation surface in felsic silicate liquids (Gualda et al. 2012) and allows for mixed H_2O-CO_2 volatile components (Ghiorso and Gualda 2015). In order to constrain the search space of models to those that might be relevant to the setting in the latest stages of post-collisional magmatism in the ANS, we selected a reference composition from the A-type Timna igneous complex studied by Litvinovsky et al. (2015), which is coeval with the Wadi Tarr magmatism and located about 185 km to the north-northeast. Timna contains no albitites. A differentiation sequence from monzogabbro through monzodiorite, monzonite, quartz monzonite and quartz syenite there ends in alkali-feldspar granites.

When testing a cumulate model for the origin of a plutonic rock, we do not expect the liquid line of descent (LLD) to pass through the whole rock composition; such a comparison of model liquids to whole-rock data is only appropriate for a testing the hypothesis that the rocks represent frozen liquid compositions. Instead, a successful model for a cumulate will show that the solids being extracted along some segment of the LLD correspond to the observed rock. Since removal of a certain solid assemblage will, by mass balance, cause the liquid composition to move away from those solids, the expectation is that the segment of the LLD where fractional extraction of the cumulate occurred should move radially away from the whole rock composition. That is, we seek a case where the whole rock composition of the cumulate plots at one end of a tangent to the LLD.

Figure 8a shows the calculated liquid lines of descent for the rhyoliteMELTS model in a total alkali-silica (TAS) diagram, as an example of a composition space where the above complementary relationship might be observed. The rhyoliteMELTS model of fractional crystallization at 200 bars pressure and the Ni-NiO oxygen buffer of monzogabbro Z333

(Supplementary Table 8; shown in blue; 47.11 wt. % SiO_2, 3.48 wt. % Na_2O, 2.95 wt. % K_2O; ASI 0.78 and AI 0.53) from Litvinovsky et al. (2015) evolves to the syenite field but then turns down towards the high-alkali tip of the granite field, encountering alkali feldspar saturation at ~950 °C and quartz saturation at ~750 °C. The late feldspar compositions approach the orthoclase endmember (Fig. 8b). The full output of all the rhyoliteMELTS runs described here are given in the Supplementary Material. Modifying this composition by lowering total alkalis by 0.5 wt. % (reducing Na_2O by 1 wt. % and increasing K_2O by 0.5 wt. %; Supplementary Table 8) yields a less alkaline monzogabbro whose evolution (shown in red) leads to the low-alkali corner of the syenite field and then turns more sharply towards the granite field.

Modifying the starting composition in the opposite direction by increasing total alkalis by 0.5 wt. % (adding 1 wt. % Na_2O and subtracting 0.5 wt. % K_2O; Supplementary Table 8) yields a more alkaline starting liquid that plots in the Foid Gabbro field (ASI 0.74 and AI 0.6; as a volcanic rock this composition would be a tephrite). The LLD of this composition (shown in green) tracks on the high-alkali side of the feldspar thermal divide, avoiding quartz saturation at any temperature. However, it also misses the alkali feldspar solvus and tracks towards pure orthoclase residual feldspars at low temperature (Fig. 8b). There is no significant segment of this LLD that plots tangent to extraction of albitite. Hence, we looked at a further modification, increasing total alkalis by yet another 0.5% (to 5.48 wt. % Na_2O and 1.95 wt. % K_2O; Supplementary Table 8) to make an even more alkaline Foid Gabbro (or tephrite) composition (ASI 0.71 and AI 0.67). This yields liquid lines of descent (shown in orange) that turn sharply upwards in the TAS diagram (Fig. 8a), moving towards a highly peralkaline hydrous sodium-silicate liquid rather than the granite minimum. They never approach quartz saturation. Furthermore, at 720 °C the LLD of this composition encounters the alkali feldspar solvus and begins to precipitate increasingly albitic feldspar (Fig. 8b). The lowest-temperature segment of this LLD also moves tangentially away from the albitite whole rock compositions in total alkali-

silica space, as shown in Fig. 8a. In fact, this LLD moves tangentially away from the albitite whole-rock compositions in *every* major element oxide vs. SiO_2 variation diagram (Supplementary Figure 1) except K_2O-SiO_2 (see below), with the points of tangency at the same temperature in every plot. Hence, this is a promising chemical model for the formation of albitite — rather than alkali feldspar granite, pegmatite, or aplite — in the cupola of the magma chamber.

We investigated the sensitivity of the calculated LLD to a number of model parameters. The result is insensitive to pressure, yielding similar results anywhere from 100 to 1000 bars (both the 200 bar and 500 bar LLDs of the most alkaline starting composition are plotted in Fig. 8a). It is insensitive to fO_2, yielding similar results at the Ni-NiO and quartz-fayalite-magnetite buffers. It is insensitive to volatile composition, yielding similar results in a pure H_2O case and with up to 2000 ppm CO_2. This last feature of the model is attractive, because the high-CO_2 cases yield albitite coexisting with both a peralkaline hydrous sodium-silicate melt and a CO_2-rich vapor that could lead to carbonate precipitation. We also note a very significant additional success of this model: only the highly alkaline Foid Gabbro starting composition yields a LLD that crystallizes both biotite and clinopyroxene, the mafic phases whose relics are found in the Wadi Tarr albitite. Finally, from a trace element perspective, all the tested models are plausible pathways to the observed patterns, fractionating abundant apatite and ilmenite to generate negative P and Ti anomalies.

None of the rhyoliteMELTS model runs reaches pure albite. The model is designed for igneous petrology and calibrated at temperatures at and above the granite minimum. Yet recent work indicates that peralkaline silicate liquids may continue to crystallize feldspars down to considerably lower temperatures than traditionally thought (e.g., Lundstrom 2016; Ackerson et al. 2018). Indeed, the final liquids in the rhyoliteMELTS runs are highly peralkaline (ASI ~ 0.1 and AI ~ 9!), most of the Al_2O_3 having been sequestered into feldspars. When the rhyoliteMELTS models terminate at ~700 °C, the last feldspar in equilibrium with the melt is $An_3Ab_{78}Or_{20}$ at 200

bars or $An_1Ab_{86}Or_{14}$ at 500 bars. The use of tangents to the liquid line of descent, which successfully matches the Wadi Tarr albitite compositions as cumulates in every oxide except K_2O, suggests that the original cumulate contained ~4.5 wt.% K_2O, which is in fact reasonably consistent with the cumulate having been dominated by alkali feldspar with ~20 mol% orthoclase component (Supplementary Figure 1). This K_2O was apparently leached out after cumulate extraction. Formation of true albitite therefore requires continued interaction between the feldspar and the residual fluids as temperature decreases below the igneous range. Such continued interaction at low temperature is strongly implied by the application of two-feldspar thermometers such as Benisek et al. (2004), wherein the coexistence of Ab>97 and Or>95 feldspars requires temperatures well below the calibrated range of the thermometer (down to ~600 °C) and likely close to ~400 °C. This late stage yields a source of K_2O to the fluids to drive K-metasomatism in the alteration zone and, finally, a nearly pure albitite. Both the magmatic evolution bringing the system close to albite end-member feldspar while avoiding the precipitation of quartz and the post-magmatic evolution transferring the residual orthoclase component to the fluids are necessary steps, and both are consistent with the observed field relations of the intrusion and its aureole.

We also emphasize that rhyoliteMELTS is an equilibrium thermodynamic model. It cannot describe important disequilibrium and dissipative process such as crystallization in a temperature gradient or physical segregation of cumulate phases by shear flows. This is important because even the most successful model considered, which is chemically consistent with origin of an igneous albitite in that it shows a path to a magmatic liquid that it is equilibrium with sodium-rich feldspar and not quartz-saturated, does not every crystallize an assemblage of pure sodic feldspar. Indeed, the final assemblage at the lowest temperature the model can reach includes biotite, magnetite, ilmenite, and potassic feldspar. All these phases may be resorbed by low-temperature processes or may be segregated from the albite by crystallization in a temperature

gradient, by shear deformation, or by density segregation. We have not modeled these physical processes and we acknowledge they are necessary. Nevertheless, the chemical consistency test that arises from the MELTS model strongly argues for the hypothesis that the albites are modified cumulates from a highly alkaline liquid.

7.3. Geodynamic model

The suggested geodynamic model for the evolution of the hypabyssal and volcanic albitites of Tarr area is shown is Fig. 9. The Wadi Tarr albitite is surrounded by an aureole of metasomatically altered rocks (fenites), explosive breccia and intrusive carbonates. This association is very reminiscent of the typical geometry of a magmatic cupola (Cloos, 2001), i.e. a spatially restricted volume at the very top of a magma chamber where low-density materials accumulate at low pressure and exsolve their volatile budget. Azer et al. (2010) concluded that the Tarr albitites formed in a magmatic cupola above an A-type granitic magma chamber but were unable to locate the position of the cupola apex due to limited field work.

The present data indicates that the two textural forms of albitite in the area formed at different levels of a magmatic cupola. We observed steeply-dipping contacts between the western, hypabyssal albitite and its country rocks in Wadi Tarr proper, whereas the intrusive contacts of the Eastern, porphyritic albitite in Wadi Ghorabi El-Hatimiya and Wadi Khashm El-Fakh are gently dipping. The geometry suggests that the cupola apex was positioned directly above the porphyritic albitite. The formation of marginal breccias is mostly confined to the porphyritic albitite, supporting explosive eruption at the cupola apex due to accumulation of gas and fluid at the roof of the magma chamber.

We propose a model in which the parent magma of the albitites was a strongly alkaline primitive magma such as tephrite, which evolved along the boundary between trachyte and phonolite before turning upwards to a highly peralkaline, hydrous sodium silicate residual liquid,

coexisting with a mixed H_2O-CO_2 fluid. An extensional tectonic regime enabled this evolving alkaline magma to ascend to a storage site in the upper crust and exsolve volatiles that concentrated at the top of the magmatic cupola. The highly alkaline nature of the evolving magma led to an unusual liquid line of descent that avoided both quartz saturation and a path towards orthoclase-rich feldspars. Nevertheless, the melt was never close to pure albite stoichiometry. After precipitating early plagioclase, ilmenite, apatite, augite, and biotite, the last precipitating feldspar at magmatic temperature was ~$Ab_{80}Or_{20}$. Some dissipative process such as crystallization in a temperature gradient or flow-induced segregation may have separated this sodium-rich feldspar from other crystallizing minerals, or those minerals may have been destabilized at low temperature in the hydrothermal regime. Continued cooling allowed exchange between the solids and residual fluids, leaving the solids nearly pure albite and exporting the orthoclase component, the carbonate component, and the low-Al_2O_3 peralkaline fluid into the aureole. This model suggests a simple answer to the question of why albitites are rare: the required highly alkaline precursor magma is also rare, though not unreasonable to find in a post-collisional A-type setting.

In the absence of exposed contacts between the hypabyssal and porphyritic members, it is difficult to say whether the cupola froze from the top downwards, with the porphyritic phase crystallizing before the underlying hypabyssal phase, or the opposite. However, it is likely that crystallization of both phases was nearly contemporaneous. The formation of the porphyritic phase beneath a gently sloping country-rock roof at the apex of the cupola, may be explained by the growth of large phenocrysts in a highly evolved, volatile-rich, magma followed by rapid development of a fine-grained matrix upon pressure quenching related to opening of fractures and sudden escape of volatiles. The presence of breccias at the margins of the porphyritic phase likely indicates an explosive eruption, although the erupted products are not preserved.

Exsolution of magmatic fluids from the ascending and crystallizing magma occurred under lithostatic pressure until the overpressure was sufficient to rupture the cupola in an explosive

event. Presumably, fluid delivery from the long-lived deeper parts of the magmatic system continued after freezing of the cupola. At various times during the evolution of the system, these fluids must have been carbonate rich, to precipitate dolomite, and water-rich, to drive formation of hydrous phases associated with the Na-metasomatism, amphibolitization, and K-metasomatism alterations. The dolomite appears to have grown from magmatically-derived carbonate-rich fluids, whereas the isotopic composition of cross-cutting breunnerite indicates a later fluid pulse that interacted with meteoric or crustal fluids, as suggested by Bogoch et al. (1986) and Azer et al. (2010).

7.4. Comparison of Tarr albitites with other Neoproterozoic albitites in the ANS

The Tarr albitites are different from those of the Eastern Desert of Egypt because of the absence of greisen formations and the presence of volcanic breccias, although albitites in the Um Ara area of the Eastern Desert are compositionally similar to the Tarr albitites (Abdalla et al. 1996). Compared to other alkali granites in southern Sinai (El-Tokhi, 2001; Azer, 2013; Khalil et al., 2018) and Israel (Mushkin et al. 2003), the Tarr albitites are distinct both in their very low modal quartz content and their distinctly lower abundances of most trace elements. In comparison with A-type syenites of the ANS (El-Tokhi, 2001; Mushkin et al., 2003; Azer, 2006; Gahlan et al., 2016), the Tarr albitites exhibit conspicuous depletions in K_2O, Fe_2O_3 and MnO contents.

According to Bentor and Eyal (1987), the Tarr albitites resemble the apogranites of the Eastern Desert of Egypt. Apogranites are greisen-bearing albitized granites of magmatic origin (e.g. Asran, 1985 in El-Gaby et al., 1988; Abou El Maaty and Ali Bik, 2000), similar in this regard to Tarr albitites. Despite considerable textural and some geochemical similarities between apogranites and the Tarr albitites, the apogranites of the Eastern Desert of Egypt are rare-metal bearing, HFSE-enriched granites (e.g. Sabet et al., 1973a,b; 1976; Helba, 1994; Abdalla et al.,

1996; Arslan et al., 1997; Abou El Maaty and Ali Bik, 2000). The lack of these characteristic enrichments in the Tarr albitites makes them a distinct type from such apogranites.

8. Conclusions

- Field study of the bodies of albitite in the Wadi Tarr region revealed that their distribution is not structurally controlled. They have intrusive contacts against the country rocks accompanied by marginal brecciation. The brecciation of the albitites and their volcanic host rocks is not related to major thrust faults as previously thought, but rather represents explosive igneous brecciation at the apex of a magmatic cupola due to exsolution of magmatic volatiles from highly evolved hydrous and carbonate-bearing peralkaline melt. The emplacement of albitite was associated with intrusion of coarsely crystalline carbonates as small dike-like bodies.
- Both the western, hypabyssal albitite and the eastern, porphyritic albitite are enveloped by pervasively altered country rocks. The breccia zones and adjacent country rocks are characterized by intensive and pervasive fenitization that accompanied emplacement of albitite. The steeply-dipping contacts of the western albitites and the shallowly-dipping to horizontal upper boundary of the eastern albitite establishes the location of the apex of the magmatic cupola of the syenitic magma chamber where the albitites developed.
- The geochemical results show that the hypabyssal and porphyritic albitites are nearly similar and closely related in their compositions. We conclude that the hypabyssal and porphyritic albitites have a common petrogenetic origin.
- Considering the challenge of generating an igneous rock that is nearly pure albite, given the tendency of metaluminous and even moderately peralkaline liquid lines of descent to lead to quartz saturation and potassium-rich feldspars, we proposed a chemical model involving fractionation from a strongly alkaline, tephritic magma. Calculations with a self-consistent crystal-melt-fluid equilibrium model show a late magmatic stage in which albite-rich feldspar,

hydrous peralkaline sodium-silicate melt, and carbonate-rich fluid can coexist. A physical segregation process may have been necessary to separate the sodic feldspar from other crystallizing phases, unless these proved soluble in later fluids. Cooling below the magmatic range would allow the pure feldspar rock to react towards endmember albitite, expelling potassic fluid that participated in the formation of the alteration aureole.

Acknowledgment

PDA and the development of the alphaMELTS2 interface to rhyoliteMELTS were funded by the US National Science Foundation through award EAR-1550934. The authors extend their appreciation to the Deanship of Scientific Research, King Saud University, for supporting this work through research group no. (RG-1436-036). We thank Craig Lundstrom for an exceptionally thoughtful review. We are also indebted to Prof. Nelson Eby (Editor in Chief) for numerous helpful comments.

References

Abdalla, H.M., Ishihara, S., Matsueda, H., Abdel Monem, A.A., 1996. On the albite-enriched granitoids Um Ara area, Southeastern Desert, Egypt. 1. Geochemical, ore potentiality and fluid inclusion studies. Journal of Geochemical Exploration 57, 127–138.

Abdelfadil, K.M., Obeid, M.A., Azer, M.K., Asimow, P.D., 2018. Late Neoproterozoic adakitic lavas in the Arabian-Nubian shield, Sinai Peninsula, Egypt. Journal of Asian Earth Sciences 158, 301–323.

Abdel-Rahman, A.M., 1994. Nature of biotites from alkaline, calc-alkaline and peraluminous magmas. Journal of Petrology 35, 525-541.

Abou El Maaty, M.A., Ali Bik, M.W., 2000. Petrology of alkali feldspar granites of Nuweibi and Gebel El-Mueilha, central Eastern Desert, Egypt. Egypt Journal of Geology 44, 127-148.

Abu El-Enen, M.M., 2008. Geochemistry and metamorphism of the Pan-African back arc Malhag volcano-sedimentary Neoproterozoic association, Wadi Kid area, southeast Sinai, Egypt. Journal of African Earth Science 51(4), 189-206.

Ackerson M.R., Mysen B.O., Tailby N.D., Watson E.B., 2018. Low-temperature crystallization of granites and the implications for crustal magmatism. Nature 559,94-97.

Akinin, V.V., Sobolev, A.V., Ntaflos, T., Richter, W., 2005. Clinopyroxene megacrysts from Enmelen melanephelinitic volcanoes (Chukchi Peninsula, Russia): application to composition and evolution of mantle melts. Contributions to Mineralogy and Petrology 150, 85-101.

Ali, B.H., 2015. SHRIMP U–Pb zircon geochronology: evidence for emplacement time of some granitoids north Eastern Desert, Egypt. Arabian Journal of Geosciences 8, 5465-5474.

Ali, B.H., Wilde, S.A., Gabr, M.M.A., 2009. Granitoid evolution in Sinai, Egypt, based on precise SHRIMP U–Pb zircon geochronology. Gondwana Research 15, 38–48.

Azer, M.K., 2013. Late Ediacaran (605-580 Ma) post-collisional alkaline magmatism in the Arabian–Nubian Shield: a case study of Serbal ring-shaped intrusion, southern Sinai, Egypt. Journal of Asian Earth Sciences 77, 203-223.

Azer, M.K., Abdelfadil, K.M., Asimow, P.D., Khalil, A.E.S., 2018. Tracking the transition from subduction-related to post-collisional magmatism in the north Arabian-Nubian Shield: A case study from the Homrit Waggat area of the Eastern Desert of Egypt. Geological Journal (accepted).

Azer, M.K., Farahat, E.S., 2011. Late Neoproterozoic volcano-sedimentary succession of Wadi Rufaiyil, southern Sinai, Egypt: a case of transition from late- to post-collisional magmatism. Journal of Asian Earth Sciences 42, 1187–1203.

Azer, M.K., Obeid, M.A., Gahlan, H.A., 2016. Late Neoproterozoic layered mafic intrusion of arc-affinity in the Arabian-Nubian Shield: A case study from the Shahira layered mafic intrusion, southern Sinai, Egypt. Geologica Acta 14, 237-259.

Azer, M.K., Obeid, M.A., Ren, M., 2014. Geochemistry and petrogenesis of late Ediacaran (580-605 Ma) post-collisional alkaline rocks from Katherina Ring complex, south Sinai., Egypt. Journal of Asian Earth Sciences 93, 229-252.

Azer, M.K., Stern, R.J., Kimura, J.-I., 2010. Origin of a Late Neoproterozoic (605±13 Ma) intrusive carbonate-albitite complex in Southern Sinai Egypt. International Journal of Earth Sciences 99, 245–267.

Be'eri-Shlevin, Y., Katzir, Y., Whitehouse M., 2009. Post-collisional tectono-magmatic evolution in the northern Arabian-Nubian Shield (ANS): Time constraints from ion-probe U-Pb dating of zircon. Journal of Geological Society 166, 71-85.

Be'eri-Shlevin, Y., Samuel, M.D., Azer, M.K., Rämö, O.T., Whitehouse, M.J., Moussa, H.E., 2011. The Ediacaran Ferani and Rutig volcano-sedimentary successions of the northernmost Arabian-Nubian Shield (ANS): New insights from zircon U–Pb geochronology, geochemistry and O–Nd isotope ratios. Precambrian Research 188, 21-44.

Benisek, A., Kroll, H., Cemič, L., 2004. New developments in two-feldspar thermometry. American Mineralogist 89, 1496-1504.

Blasband, B., Brooijmans, P., Dirks, P., Visser, W., White, S., 1997. A Pan-African core complex in the Sinai, Egypt. Geologie en Mijnbouw 76, 247–266.

Blasband, B., White, S., Brooijmans, P., De Boorder, H., Visser, W., 2000. Late Proterozoic extensional collapse in the Arabian–Nubian Shield. Journal of the Geological Society of London 157, 615–628.

Blasy, M., Baroudy, A.F., Kharbish, S.M., 2001. Geochemical characteristics of Wadi Tarr albitite, Southeastern Sinai, Egypt. Egyptian Journal of Geology 42, 767–780.

Bogoch, R., Magaritz, M., Michard, A., 1986. Dolomite of possible mantle origin, Southeast Sinai. Chemical Geology 56, 281–288.

Bogoch, R., Bahat, D., Kisch, H., 1987. The Tarr albitite: a metasomatic plagiogranite from mainly non-intrusive protoliths. Ofioliti 12, 8–22.

Boskabadi, A., Pitcairn, I.K., Stern, R.J., Azer, M.K., Broman, C., Mohamed, F.H., Majka, J. 2013. Carbonatite crystallization and alteration in the Tarr carbonatite-albitite complex, Sinai Peninsula, Egypt. Precambrian Research 239, 24-41.

Brooijmans, P., Blasband, B., White, S.H., Visser, W.J., Dirks, P., 2003. Geothermobarometric evidence for a metamorphic core complex in Sinai, Egypt. Precambrian Research 123, 249-268.

Brooker, E.A., Hamilton D.L., 1990. Three-liquid immiscibility and the origin of carbonatites. Nature 346, 459-462.

Bucholz C.E., Jagoutz O., Schmidt M.W., Sambuu O., 2014a. Phlogopite-and clinopyroxene-dominated fractional crystallization of an alkaline primitive melt: petrology and mineral chemistry of the Dariv Igneous Complex, Western Mongolia. Contributions to Mineralogy and Petrology 167(4), 994.

Bucholz C.E., Jagoutz O., Schmidt M.W., Sambuu O., 2014b. Fractional crystallization of high-K arc magmas: biotite-versus amphibole-dominated fractionation series in the Dariv Igneous complex, Western Mongolia. Contributions to Mineralogy and Petrology 168(5), 1072.

De la Roche, H., Leterrier, J., Grandclaude, P., Marchal, M., 1980. A classification of volcanic and plutonic rocks using R_1-R_2 diagrams and major-element analyses-Its relation with current nomenclature. Chemical Geology 29, 183-210.

El-Bialy, M.Z., 2010. On the Pan-African transition of the Arabian–Nubian Shield from compression to extension: The post-collision Dokhan volcanic suite of Kid-Malhak region, Sinai, Egypt. Gondwana Research 17(1), 26-43.

El-Bialy, M.Z., 2013. Geochemistry of the Neoproterozoic metasediments of Malhaq and Um Zariq formations, Kid metamorphic complex, Sinai, Egypt: Implications for source-area weathering, provenance, recycling, and depositional tectonic setting. Lithos 175–176, 68-85.

El-Gaby, S., Khudeir, A.A., Abdel Tawab, M., Atalla, R.F., 1991. The metamorphosed volcano sedimentary succession of Wadi Kid, southeastern Sinai, Egypt. Annals of Geological Survey of Egypt 17, 19-35.

Eliwa, H.A., Abu El-Enen, M.M., Khalaf, I.M., Itaya, T., Murata, M., 2008. Metamorphic evolution of Neoproterozoic metapelites and gneisses in the Sinai, Egypt: insights from petrology, mineral chemistry and K-Ar age dating. Journal of African Earth Sciences 51, 107-122.

Elliott, H.A.L., Wall, F., Chakhmouradian, A.R., Siegfried, P.R., Dahlgren, S., Weatherley, S., Finch, A.A., Marks, M.A.W., Dowman, E., Deady, E., 2018. Fenites associated with carbonatite complexes: A review. Ore Geology Reviews 93, 38-59.

El-Metwally, A.A., El-Aasy, I.E., Ibrahim, M.E., Essawy, M.A., El-Mowafy, A.A., 1999. Petrological, structural and geochemical studies on the basement rocks of Gabal Um- Zariq-Wadi Kid area, South Eastern Sinai. Egyptian Journal of Geology 43(1), 147-180.

El-Shazly, S.M., M.A. Hassanen, 1989. Petrochemistry and petrogenesis of the Younger Granitoids, Wad Kid area, Sinai, Egypt. 1st International conference of Geochemistry, Alexandria University, Egypt, pp: 83-103.

El-Tokhi, M., 2001. Petrogenesis and geochemistry of some quartz syenites from Southern Sinai, Egypt. The second International Conference on the Geology of Africa, Assiut University, Egypt, 239-253.

Evensen, N.M., Hamilton, P.J., O'Nions, R.K., 1978. Rare earth abundances in chondritic meteorites. Geochimica et Cosmochimica Acta 42, 1199–1212.

Eyal, M., Be'eri-Shlevin, Y., Eyal, Y., Whitehouse, M.J., Litvinovsky, B., 2014a. Three successive Proterozoic island arcs in the Northern Arabian–Nubian Shield: Evidence from SIMS U-Pb dating of zircon. Gondwana Research 25(1), 338-351.

Eyal, M., Zanvilevich, A.N., Litvinovsky, B.A., Jahn, B.M., Vapnik, Ye., Be'eri-Shlevin, Y. 2014b. The Katherina ring complex (Sinai Peninsula, Egypt): Sequence of emplacement and petrogenesis. American Journal of Science 314, 462-507.

Farahat, E.S., Azer, M.K., 2011. Post-collisional magmatism in the northern Arabian-Nubian Shield: the geotectonic evolution of the alkaline suite at G. Tarbush area, south Sinai, Egypt. Chemie der Erde 71, 247-266.

Furnes, H., Shimron, A.E., Roberts, D., 1985. Geochemistry of Pan- African volcanic arc sequences in southeastern Sinai Peninsula and plate tectonic implications. Precambrian Research 29, 359-382.

Gahlan, H.A., Azer, M.K., Asimow, P.D., Al-Kahtany, K., 2016. Late Ediacaran post-collisional A-type syenites with shoshonitic affinities, northern Arabian-Nubian Shield: A possible mantle-derived A-type magma. Arabian Journal of Geosciences 9, 613(doi:10.1007/s12517-016-2629-x).

Ghabrial, D.S., Alibik, M.W., Abdelwahab W., 2013. Albitites of Tarr Complex, Kid area, southeastern Sinai: petrology, geochemistry and petrogenesis. Journal of Applied Sciences Research 9, 4443-4462.

Ghiorso M.S., Sack R.O., 1995. Chemical mass transfer in magmatic processes IV. A revised and internally consistent thermodynamic model for the interpolation and extrapolation of liquid-solid equilibria in magmatic systems at elevated temperatures and pressures. Contributions to Mineralogy and Petrology 119(2-3), 197-212.

Ghiorso M.S., Gualda G.A.R., 2015. An H_2O–CO_2 mixed fluid saturation model compatible with rhyolite-MELTS. Contributions to Mineralogy and Petrology 169, 53.

Girardeau, J. Mevel, C., 1982. Amphibolitized sheared gabbros from ophiolites as indicators of the evolution of the oceanic crust: Bay of islands, Newfoundland. Earth Planetary Science Letter 61, 151-165.

Grove, T. L., Elkins Tanton, L. T., Parman, S. W., Chatterjee, N., Müntener, G., Gaetani, G. A., 2003. Fractional Crystallization and Mantle Melting Controls on Calc-Alkaline Differentiation Trends. Contributions to Mineralogy and Petrology, 145(5), 515-533.

Gualda G.A.R., Ghiorso M.S., Lemons R.V., Carley T.L., 2012. Rhyolite-MELTS: a Modified Calibration of MELTS Optimized for Silica-rich, Fluid-bearing Magmatic Systems. Journal of Petrology 53(5), 875-890.

Hafez, A.M.A., Abdel Wahed, M., Shallaly, N.A., 2007. Microfabric, geochemistry and clockwise P-T path of the Precambrian metasediments in the central Wadi Kid area, Southeastern Sinai. In: The 15th Symposium on Precambrian and development (abstract), Cairo, Egypt.

Heinrich, E. W., 1966. The Geology of Carbonatites. Rand McNally, Chicago. 555p.

Johnson, D. M., Hooper, P. R., Conrey R. M., 1999. XRF Analysis of Rocks and Minerals for Major and Trace Elements on a Single Low Dilution Li-tetraborate Fused Bead. Advances in X-ray Analysis 41, 843-867.

Katzir, Y., Eyal, M., Litvinovsky, B.A., Jahn, B.M., Zanilevich, A.N., Valley, J.W., Beeri, Y., Shimshilashvili, E., 2007. Petrogenesis of A-type granites and origin of vertical zoning in the Katharina pluton, Gebel Mussa (Mt Moses) area, Sinai, Egypt. Lithos 95, 208–228.

Keeditse, M. Rajesh, H.M., Belyanin, G.A., Fukuyama, M., Tsunogae, 2016. Primary magmatic amphibole in Archaean meta-pyroxenite from the central zone of the Limpopo Complex, South Africa. South African Journal of Geology 119(4), 607-622.

Khalifa, I.H., El-Bialy, M.Z., Hassan, D.M., 2011. Petrologic and geochemical characterization and mineralization of the metavolcanic rocks of the Heib Formation, Kid Metamorphic Complex, Sinai, Egypt. Geoscience Frontiers 2(3), 385-402.

Khalil, A.E.S., Obeid, M.A., Azer, M.K., Asimow, P.D., 2018. Geochemistry and petrogenesis of post-collisional alkaline and peralkaline granites of the Arabian-Nubian Shield: a case study from the southern tip of Sinai Peninsula, Egypt. International Geology Review 60(8), 998-1018.

Kinnaird, J.A., Bowden, P., 1991. Magmatism and mineralisation associated with Phanerozoic Anorogenic Plutonic Complexes of the African Plate. In Kampunzu A. and Lubala R. T., eds. Magmatism in Extensional Structural Settings: the Phanerozoic African Plate, pp. 410-485. Springer-Verlag, Berlin.

Le Bas, M.J., 1962. The role of aluminium in igneous clinopyroxenes with relation to their parentage: American Journal of Science 260, 267–288.

Leake, B.E., Woolley, A.R., Arps, C.E.S., Birch, W.D., Gilbert, M. C., Grice, J.D., Hawthorne, F.C., Kato, A., Kisch, H. J., Krivovichev, V.G., Linthout, K., Laird, J., Mandarino, J., Maresch, W.V., Nickel, E.H., Rock, N.M.S., Schumacher, J.C., Smith, D.C., Stephenson, N.C.N., Ungaretti, L., Whittaker, E.J.W., Youzhi, V., 1997. Nomenclature of amphiboles: Report of the Subcommittee on Amphiboles of the International Mineralogical Association Commission on New Minerals and Mineral Names. Mineralogical Magazine 61, 295-321.

Leterrier, J., Maury, R.C., Thonon, P., Girard, D., Marchal, M., 1982. Clinopyroxene composition as a method of identification of the magmatic affinities of paleo-volcanic series. Earth and Planetary Science Letters 59, 139–154.

Liégeois, J.P., Black, R., 1987. Alkaline magmatism subsequent to collision in the Pan-African belt of the Adrar des Iforas. In: Fitton, J.G., Upton, B.G.J. (Eds.), Alkaline Igneous Rocks. Geological Society, Special Publication 30, 381-401.

Liégeois, J.P., Navez, J., Black, R., Hertogen, J., 1998. Contrasting origin of post-collision high-K calc-alkaline and shoshonitic versus alkaline and peralkaline granitoids. The use of sliding normalization. Lithos 45, 1-28.

Lindsley, D.H., 1983. Pyroxene thermometry. American Mineralogist 18, 477-493.

Litvinovsky, B.A. Jahn, B.M., Eyal, M., 2015. Mantle-derived sources of syenites from the A-type igneous suites-New approach to the provenance of alkaline silicic magmas. Lithos 232, 242–265.

Lundstrom, C.C., 2016. The role of thermal migration and low- temperature melt in granitoid formation: can granite form without rhyolitic melt? International Geology Review 58(3): 371-388.

Mark, G., 2007. Albitite formation by selective pervasive sodic alteration of tonalite plutons in the Cloncurry district, Queensland. Australian Journal of Earth Sciences 45 (5), 765-774.

Middlemost E.A.K., 1994, Naming materials in the magma/igneous rock system. Earth-Science Reviews 37(3-4):215-224.

Moghazi, A.M., Ali, K.A., Wilde, S.A., Zhou, Q., Andersen, T., Andresen, A., Abu El-Enen, M.M., Stern, R.J., 2012. Geochemistry, geochronology, and Sr-Nd isotopes of the Late Neoproterozoic Wadi Kid volcano-sedimentary rocks, Southern Sinai, Egypt: implications for tectonic setting and crustal evolution. Lithos 154(1), 147-165.

Moghazi, A.M., Anderson, T., Oweiss, G.A., El Bouselly, A.M., 1998. Geochemical and Sr-Nd-Pb isotopic data bearing on the origin of Pan-African granitoids in the Kid area, southeast Sinai, Egypt. Journal of the Geological Society of London 155(4), 697-710.

Moreno, J.A., Molina, J.F., Montero, P., Abu Anbar, M., Scarrow, J.H., Cambeses, A., Bea, F 2014. Unraveling sources of A-type magmas in juvenile continental crust: Constraints from compositionally diverse Ediacaran post-collisional granitoids in the Katerina Ring Complex, southern Sinai, Egypt. Lithos 192-195, 56-85.

Moussa, E.M.M., Stern, R.J., Manton, W.I., Ali, K.A., 2008. SHRIMP zircon dating and Sm/Nd isotopic investigations of Neoproterozoic granitoids, Eastern Desert, Egypt. Precambrian Research 160, 341-356.

Mushkin, A., Navon, O., Halicz, L., Heimann, A., Hartmann, G., Stein, M., 2003. The petrogenesis of A-type magmas from the Amram Massif, southern Israel. Journal of Petrology 44, 815–832.

Nachit, H., Ibhi, A., Abia, E.H., Ohoud, M.B., 2005. Discrimination between primary magmatic biotites, reequilibrated biotites and neoformed biotites. Comptes Rendus Géoscience 337, 1415-1420.

Nisbet, F.G., Pearce, J.A., 1977. Clinopyroxene composition in mafic lavas from different tectonic settings. Contribution to Mineralogy and Petrology 63, 149–160.

Obeid, M.A., Azer, M.K., 2015. Pan-African adakitic rocks of the north Arabian-Nubian Shield: petrological and geochemical constrains on the evolution of the Dokhan volcanics in the north Eastern Desert of Egypt. International Journal of Earth Sciences 104, 541-563.

Pearce, J. A, Harris, N. B. W., Tindle, A.G., 1984. Trace element discrimination diagrams for the tectonic interpretation of granitic rocks. Journal of Petrology 25, 956-83.

Pearce, J.A., 1983. Role of the sub-continental lithosphere in magma genesis at active continental margins. In: Hawkesworth, C.J., Norry, M.J. (Eds.), Continental Basalts and Mantle Xenoliths. Shiva, Nantwich, pp. 230-249.

Pin, C., Monchoux, P., Paquette, J- L., Azambre, B., Wang, R.C., Martin, R.F., 2006. Igneous albitite dikes in orogenic lherzolites, western Pyrenees, France: A possible source for corundum and alkali feldspar xenocrysts in basaltic terranes. II. Geochemical and petrogenetic considerations. The Canadian Mineralogist 44 (4), 843-856.

Reymer, A.P.S., 1983. Metamorphism and tectonics of Pan-African terrain in Southeastern Sinai. Precambrian Research 19, 225–238.

Rietmeijer, F.J.M., 1983. Chemical distinction between igneous and metamorphic orthopyroxenes especially those coexisting with Ca-rich clinopyroxenes: A reevaluation. Mineralogical Magazine 47, 143–51.

Sabet, A.H., Chabanenco, V., Tsogoev, V., 1973a. Tin-tungsten and rare-metal mineralization in the central Eastern Desert of Egypt. Annals of Geological Survey of Egypt 3, 75-86.

Sabet, A.H., Tsogoev, V., 1973b. Problems of geological and economic evolution of tantalum deposits in apogranites during stages of prospection and exploration. Annals of Geological Survey of Egypt, 3, 87-108.

Sabet, A.H., Tsogoev, V.B., Babourin, L.M., Riad, A.M., Zakhari, A., Armanius, L.K., 1976. Geologic structure and laws of localization of tantalum mineralization at the Nuweibi deposit. Annals of Geological Survey of Egypt 6, 119-156.

Shahien, M.G., 2002. Petrochemistry and petrogenesis of Kid granitoids, South Eastern Sinai, Egypt. 6th International Conference on Geology of Arab World, Cairo University, 101-118.

Shimron, A.E., 1975. Petrogenesis of the Tarr albitite–carbonatite complex, Sinai Peninsula. Mineralogical Magazine 40, 13–24.

Shimron, A.E., 1980. Proterozoic island arc volcanism and sedimentation in Sinai. Precambrian Research 12, 437–458.

Shimron, A.E., 1984. Evolution of the Kid Group, southeast Sinai Peninsula: thrusts, mélanges, and implications for accretionary tectonics during the Proterozoic of the Arabian- Nubian Shield. Geology, 12(4), 242-247.

Soliman, K.A., Tolba, M.E., El-Manakhly, M.M., Madbouly, M.E., Hasan, M.M., Abd El Magid, E.A., Khyamy, A.A., Abd El Mola, A.F., Mohamed, H.A., 1992. Geology of the albitite rock, Wadi El-Tarr, Southern Sinai. Annals of Geological Survey of Egypt 18, 29–37.

Whalen, J.B., Currie, K.L., Chappel, B.W., 1987. A-type granites: geochemical characteristics, discrimination and petrogenesis. Contribution to Mineralogy and Petrology 95, 407-419.

Wilson, M., 1989. Igneous Petrogenesis. Unwin Hyman, London. 457 pp.

Zharikov, V.A., Pertsev, N.N., Rusinov, V.L., Callegari, E., Fettes, D.J., 2007. Metasomatism and metasomatic rocks. In: Recommendations by the IUGS Subcommission on the Systematics of Metamorphic Rocks. British Geological Survey.

Figure captions

Figure 1. (a) Geological map of Sinai (modified after Eyal et al., 1980) with inset showing the location of the Sinai Peninsula at the northernmost extent of Neoproterozoic exposures of the Arabian-Nubian Shield. Location of the Tarr albitite within the Kid Metamorphic Complex is marked a square. (b) Simplified geological map of the study area (after Blasy et al., 2001; Azer et al., 2010).

Figure 2. Field photographs: (a) General view showing the light-colored albitite surrounded by volcanic country rocks. (b) Sharp intrusive contact of the hypabyssal albitite in a mined area. (c) Offshoot veins of intrusive albitite cross-cutting the country rocks. (d) Hypabyssal albitite at Wadi Tarr with nearly vertical intrusive contact. (e) Porphyritic albitite with shallowly-dipping upper contact. (f) Porphyritic albitite offshoots permeating the country rocks. (g) Nearly vertical intrusive contact between hypabyssal albitite and volcanics with fenite margin. (h) Sharp contact between albitite-breccia and volcanic-breccia. (i) Jigsaw-fit angular fragments of albitite clasts in a matrix of dark green fibrous amphiboles and brown carbonates. (j) Dyke of intrusive carbonate within the breccia zone.

Figure 3. Photomicrographs: (a, b) Prismatic albite phenocrysts in porphyritic albitite showing simple twinning and/or albite-Carlsbad twinning. (c) Microphenocryst of clinopyroxene altered along the margins into secondary amphiboles. (d) Anhedral biotite crystal in the hypabyssal albitite.

(e) Coarsely crystalline fibers of actinolite in the albitite breccia. (f) Secondary amphiboles forming fibrous interfragmental cement in the albitite breccia. (g) Fine aggregates of sodic amphiboles filling nests in the albitite breccia. (h) Highly sericitized andesitic rock fragments in the volcanic breccia. (i) Vug filled with secondary epidote in the volcanic breccia. (j) Crystal fragment of plagioclase completely replaced by sericite and muscovite in the altered volcanic country rock. (k) Patches of secondary albite associated with muscovite in the altered volcanic country rock; (l) Overgrowth of secondary albite around primary plagioclase.

Figure 4. Mineral chemistry diagrams: (a) Classification diagram for clinopyroxene minerals (Morimoto et al. 1988); temperature estimation contours after Lindsley (1983). (b) TiO_2–$FeO_{(t)}$–MgO ternary discrimination diagram for biotite (Nachit et al., 2005). (c) $FeO_{(t)}$ vs. Al_2O_3 biotite discriminant diagram (Abdel-Rahman, 1994). (d) Classification of amphibole on the basis of Si and $Mg/(Mg+Fe^{2+})$ (Leake et al., 1997). (e) Discrimination diagram for primary and secondary amphibole, Si vs. Ca+Na+K (after Keeditse et al., 2016)

Figure 5. Whole-rock geochemistry of the albitites: (a) Plutonic nomenclature using the R1-R2 discrimination diagram of De la Roche et al. (1980). (b) Ga/Al vs. Nb diagram of Whalen et al. (1987). (c) MORB-normalized spider diagram. (d) Chondrite-normalized REE patterns. MORB and chondrite normalization values after Pearce (1983) and Evensen et al. (1978), respectively.

Figure 6. Whole-rock geochemistry of the volcanic country rocks and rhyolitic dikes: (a) Immobile-element volcanic nomenclature scheme suggested by Winchester and Floyd (1977). (b) MORB-normalized spider diagram. (c) Chondrite normalized REE patterns . (d) Comparison between the chondrite normalized REE patterns of the high-silica rock labeled albitite by Ghabrial et al. (2003) and the rhyolitic dyke of the present work. MORB and chondrite normalization values after Pearce (1983) and Evensen et al. (1978), respectively.

Figure 7. SiO_2-variation diagrams showing chemical differences between altered and unaltered volcanic country rocks.

Figure 8. RhyoliteMELTS 1.1 models of magmatic differentiation of primitive A-type magmas, distinguishing those that might form albitite from those that end in granite. (a) Total alkali-silica diagram with plutonic nomenclature and field boundaries (black) from Middlemost (1994). Colored medium-weight curves show liquid lines of descent (LLDs) at 200 bars and the NNO buffer calculated with rhyoliteMELTS. The heavy curve shows the LLD of the most alkaline case at 500 bars pressure. Kinks in the less alkaline LLD trends at the appearances of alkali feldspar and quartz are indicated. The whole rock compositions of the hypabyssal and porphyritic albitites of Wadi Tarr are plotted, along with light dashed arrows indicating the segments of the most alkaline LLDs at 200 bars and 500 bars that move tangentially away from the albitite whole-rocks, indicating that they are possible complementary cumulates to the evolution of the LLDs near the tangency points. (b) Ternary Or-Ab-An diagram showing evolution of feldspar compositions in the same fractional crystallization models shown in (a), with matching colors and line weights. The dashed segments represent jumps from plagioclase fractionation to alkali feldspar fractionation. Only the most alkaline trend (orange) encounters the alkali feldspar solvus and crystallizes albitic compositions, both at 200 bars (light curves) and 500 bars (heavy curves) total pressure.

Figure 9. (a) Schematic cross-section showing the outcrop-scale relationship between the albitites, explosive breccias, intrusive carbonate and their country rocks. (b) Schematic cross-section of the Tarr magmatic-hydrothermal system showing formation of porphyritic albitite in the apex of a magmatic cupola above hypabyssal albitite.

Supplementary Figure 1. SiO_2 variation diagrams for all major oxides showing the same calculated liquid lines of descent from rhyoliteMELTS as in Fig 8a as well as the whole-rock

compositions of the two classes of Wadi Tarr albitites (symbols as in Fig 8). The two dashed arrows in each panel show the complementary relationship of the whole-rock cumulate compositions to the evolution of the liquid lines of descent of the most alkaline composition, calculated at 200 and at 500 bars, respectively. In all oxides except K_2O, the average Wadi Tarr albitite composition plots at the end of a tangent line to common points (at ~64.2% wt. % SiO_2 in the liquid for 500 bars, or 66.2 wt. % SiO_2 for 200 bars), just as in the total alkali-silica plot (Fig. 8a). There are only two exceptions: (1) the very low K_2O contents of the rocks suggest later leaching of potassium. In fact, extrapolation of the LLD tangent arrows to the SiO_2 contents of the Wadi Tarr albitites suggests that the cumulates originally contained ~4.5 wt.% K_2O (blue ellipse in the K_2O-SiO_2 plot), which is similar to the expected K_2O content of a monomineralic rock containing only $Ab_{80}Or_{20}$ alkali feldspar. (2) The P_2O_5 trend of the 500 bar LLD model is not radial from the albitite compositions at the same SiO_2 content as the other oxides. This is perhaps the only basis (and it is a weak basis, given the possibly unreliable calibration of apatite saturation in rhyoliteMELTS) for preferring the 200 bar model.

Table 1. Major oxides, some trace elements and CIPW for porphyritic and hypabyssal albitites of Tarr area.

Sample	Porphyritic albitite						Hypabyssal albitite						
	EA1	EA11	EA18	EA22	EA7	EA14	WA-14	WA-18	WA-2	WA-21	WA-24	WA-9	WA-27
	Major oxides (wt.%)												
SiO2	67.21	69.27	68.56	68.37	68.21	68.25	66.93	67.95	68.45	66.51	67.67	67.26	67.64
TiO2	0.33	0.36	0.41	0.3	0.35	0.32	0.28	0.35	0.29	0.41	0.33	0.32	0.37
Al2O3	19.66	18.83	19.18	19.28	19.44	19.37	20.01	19.01	18.86	20.16	19.55	19.45	19.57
Fe2O3	0.42	0.39	0.29	0.36	0.42	0.34	0.33	0.51	0.32	0.31	0.36	0.41	0.35
MnO	0	0.01	0	0.01	0	0.01	0.01	0.02	0.01	0	0.01	0	0.01
MgO	0.08	0.04	0.02	0.03	0.01	0.05	0.02	0.48	0	0.22	0.37	0.05	0.19
CaO	0.36	0.41	0.29	0.54	0.59	0.39	0.58	0.59	0.34	0.54	0.46	0.61	0.44
Na2O	10.82	10.29	10.86	10.08	10.3	10.74	11.13	9.96	11.04	11.01	10.23	10.68	10.56
K2O	0.21	0.2	0.18	0.27	0.13	0.31	0.17	0.23	0.13	0.34	0.29	0.17	0.25
P2O5	0.15	0.14	0.09	0.23	0.34	0.21	0.22	0.21	0.16	0.21	0.17	0.26	0.22
LOI	0.15	0.08	0.11	0.09	0.11	0.17	0.21	0.29	0.14	0.22	0.15	0.17	0.21
Total	**99.39**	**100**	**99.99**	**99.56**	**99.9**	**100.2**	**99.89**	**99.6**	**99.74**	**99.93**	**99.59**	**99.38**	**99.81**

	Trace elemnts (ppm)												
Ni	17.4	6.2	5.4	7.1	16.5	11.3	19.1	16.8	11.3	14.8	11.9	13.4	15.1
Cr	40.1	8.7	19	6.2	34.2	18.6	37.5	31.2	11.2	34.2	29.8	12.5	24.6
V	24.2	14.5	16.3	19.5	17.8	19.4	23.6	31.7	20.2	24.3	25.1	21.4	22.3
Ba	42.1	22.1	32	35.9	35.3	35.8	54.2	79.8	61.4	80.6	85.2	47.7	68.5
Rb	3.5	5.2	3.7	6.7	3	4.7	2.7	5.7	3.2	6.3	5.6	4.3	4.8
Sr	84.5	71.2	74.9	81.2	76.3	76.6	104.7	126.5	118	96.6	88.9	88.3	102.1
Zr	212.4	168.9	163.4	196.3	201.7	194.5	313.6	281.6	297.6	328.7	302.5	302.4	298.6
Y	23.8	18.9	20.7	22.6	18.4	21.1	30.6	28.3	35.1	25.4	29.7	32.3	31.2
Nb	22.3	19.3	18.4	17.8	19.9	18.9	33.6	26.5	24.5	26.6	21.6	25.4	26.8
Ga	21.7	23.6	26.7	22.9	24.5	23.6	25.6	20.8	23.4	23.6	24.1	25.2	23.4
Cu	10	9.3	10.1	8.2	10	10.2	10	5.6	7.4	5.5	6.1	6.5	7.2
Zn	26	16.7	21.2	16.3	212	61.5	22.1	14.1	20.1	8.9	6.9	18.9	13.6
Pb	5.1	2.2	1.1	2.1	4.3	3.5	3.9	2.9	4.3	3.2	7.8	3.9	5.4
	CIPW												
Quartz	2.83	7.94	4.21	8.03	7.31	4.12	0.73	7.8	3.32	0.16	5.87	3.68	4.52
Corundum	1.34	1.3	0.8	1.98	2.09	1.15	0.98	1.81	0.32	1.2	1.98	1.21	1.65
Orthoclase	1.25	1.18	1.07	1.6	0.77	1.83	1.01	1.37	0.77	2.02	1.72	1.01	1.48
Albite	92.28	87.12	92.02	85.76	87.36	90.9	94.5	84.38	93.81	93.45	87.07	91.11	89.73
Anorthite	0.81	1.12	0.85	1.18	0.71	0.56	1.45	1.57	0.65	1.31	1.18	1.34	0.75
Hypersthene	0.62	0.48	0.27	0.44	0.43	0.45	0.38	1.2	0.32	0.79	1.28	0.53	0.8
Magnetite	0.16	0.17	0.15	0.15	0.17	0.15	0.14	0.15	0.14	0.16	0.15	0.16	0.16
Hematite	-	-	-	-	-	-	-	0.03	-	-	-	-	-
Ilmenite	-	-	-	-	-	-	-	0.67	-	-	-	-	-
Apatite	0.33	0.31	0.2	0.5	0.74	0.46	0.48	0.46	0.35	0.46	0.37	0.57	0.48
	Some geochemical parameters												
AI	0.92	0.91	0.94	0.88	0.88	0.93	0.92	0.88	0.97	0.92	0.88	0.91	0.90
ASI	1.05	1.05	1.03	1.08	1.07	1.03	1.02	1.07	1.00	1.03	1.09	1.03	1.06
R1	566	893	649	880	835	642	450	882	592	422	755	628	678
R2	428	416	408	441	445	424	456	474	406	464	459	449	440
Colour Index	0.78	0.65	0.42	0.59	0.6	0.6	0.52	2.05	0.45	0.95	1.43	0.69	0.96
Diff. Index	96.36	96.23	97.29	95.4	95.44	96.86	96.24	94.06	97.9	95.62	94.66	95.8	95.73
Q	3	8	4	8	8	4	1	8	3	0.17	6	4	5
ANOR	39	49	44	42	48	23	59	53	46	39	41	57	34

Table2. REE and some trace elements for porphyritic and hypabyssal albitites of Tarr area.

	Porphyritic albitite				Hypabyssal albitite			
Sample No	EA1	EA11	EA18	EA14	WA-14	WA-2	WA-21	WA-27
	REE							
La	19.8	27.5	17.94	21.1	26.6	36.9	23.2	31.9
Ce	44.5	57.2	41.63	48.7	62.5	79.8	54.1	69.7
Pr	6.72	7.58	6.01	7.21	7.99	10.94	7.45	9.28
Nd	27.9	32.1	25.63	29.6	34.3	42.27	30.1	37.7
Sm	5.41	5.73	5.71	6.27	6.13	7.96	6.39	6.92
Eu	1.16	1.18	1.38	1.47	1.14	1.15	1.54	1.25
Gd	4.69	4.46	5.61	5.66	4.71	5.16	6.07	4.61

Tb	0.7	0.65	0.83	0.87	0.66	0.75	0.92	0.67
Dy	4.28	3.69	4.82	4.95	3.54	4.01	5.15	3.62
Ho	0.87	0.77	0.98	1.01	0.73	0.86	1.05	0.76
Er	2.54	2.34	2.83	2.92	2.21	2.43	3.01	2.24
Tm	0.39	0.35	0.42	0.45	0.33	0.36	0.47	0.33
Yb	2.64	2.48	2.89	3.02	2.24	2.42	3.13	2.28
Lu	0.4	0.37	0.44	0.46	0.34	0.36	0.49	0.34
∑REE	**122**	**146**	**117**	**134**	**153**	**195**	**143**	**172**
	Some trace elements							
Be	1.7	2.3	1.2	1.5	2.1	2.4	2.1	1.9
Co	3.8	1.6	3.2	2.1	2.2	3.1	2.7	2.6
Cs	0.1	0.4	0.1	0.2	0.3	0.2	0.2	0.1
Hf	8.2	9.4	4.3	7.9	7.4	7.4	5.4	7.3
Sn	2.8	2.2	2.5	1.8	3.2	2.1	3.1	2.4
Ta	1	1.2	1.3	1.2	1.3	1.3	1.2	1.3
Th	6.1	7.2	5.6	5.2	9.4	7.6	4.7	6.5
U	1.5	1.8	1.3	1.3	1.6	1.4	1.1	1.4
W	0.9	1.4	0.8	1.6	1.7	1.4	1.6	1.8
Mo	0.1	0.1	0.3	0.1	0.3	0.2	0.1	0.3
	Some parameters							
Eu/EU*	0.70	0.71	0.75	0.75	0.65	0.55	0.76	0.68
((La/Sm)n	2.31	3.03	1.98	2.12	2.74	2.93	2.29	2.91
(Gd/Lu)n	1.44	1.48	1.56	1.51	1.70	1.76	1.52	1.66
(La/Lu)n	5.07	7.62	4.18	4.70	8.02	10.50	4.85	9.61

Table 3. Major oxides, trace elements and REE of the country volcanic rocks .

	Rhyolitic dykes		Altered volcanics					Unaltered volcanics				
Sample	TRD-1	TRD-2	TV3	TV6	TV9	TV1	TV12	TV15	TV17	TV20	TV22	TV25
	Major oxides (wt.%)											
SiO2	73.82	74.02	62.52	61.23	63.13	62.28	61.34	63.23	61.77	62.76	61.82	60.97
TiO2	0.27	0.24	0.81	0.67	0.79	0.73	0.67	1.01	0.86	0.93	0.87	1.08
Al2O3	13.45	14.07	15.99	15.99	15.73	15.73	16.22	15.87	16.75	16.18	16.51	16.15
Fe2O3	0.48	0.35	2.95	4.2	5.03	5.27	4.29	6.09	5.23	6.23	6.24	6.97
MnO	0.03	0.02	0.05	0.06	0.04	0.04	0.08	0.03	0.05	0.08	0.07	0.11
MgO	0.72	0.64	5.21	5.05	3.87	3.98	4.25	2.18	2.13	2.46	2.65	3.13
CaO	0.54	0.47	3.98	2.07	2.04	2.19	2.89	0.95	2.55	2.23	1.9	2.43
Na2O	7.37	8.01	5.23	6.02	5.11	6.21	6.03	4.8	4.59	3.59	4.82	3.91
K2O	2.81	2.07	1.66	2.7	2.34	2.26	2.76	4.3	4.4	4.0	3.8	3.6
P2O5	0.04	0.03	0.17	0.14	0.18	0.2	0.14	0.21	0.16	0.22	0.17	0.23
LOI	0.43	0.37	2.11	1.82	2.06	1.54	1.98	0.96	1.52	1.11	1.28	1.17
Total	99.96	100.29	100.68	99.95	100.32	100.43	100.65	99.59	100.05	99.76	100.11	99.76
	Trace elemnts (ppm)											
Ni	2.7	1.2	6.4	36.7	41.1	57.8	32.3	35.6	29.5	35.4	47.8	46.7
Cr	3.9	2.2	84.2	101.2	116.7	95.6	88.9	111.2	93.4	77.8	102.1	95.6
V	6.7	16.3	113.4	98.4	123.3	99.8	134.1	85.6	106.7	95.6	113.4	94.5
Ba	41.3	51.6	124.5	246.2	135.6	223.4	187.3	452.6	578.9	656.2	708.1	527.8
Rb	91.6	101.2	17.8	36.4	41.2	27.8	43.1	48.3	31.6	113.2	91.4	64.5
Sr	111.8	146.7	113.3	151.2	98.7	102.6	133.3	457.8	387.2	391.8	406.7	564
Zr	233.7	323.4	126.6	125.7	117.4	97.4	121.4	219.2	183.5	246.7	176.4	189.4

Y	24.1	32.3	21.2	18.6	19.4	16.6	20.2	22	16.7	28.9	20.1	19.2
Nb	10.5	13.7	7.4	8.1	6.4	5.6	7.1	10.1	8.7	14.5	9.9	9.8
Ga	14.5	16.6	65.1	17.8	19.5	17.5	22.2	22.8	19.1	24.2	23.6	21.8
Cu	4.3	6.8	27.2	21.4	32.3	30.7	41.3	70.5	84.1	62.6	53.4	46.9
Zn	19.4	21.7	33.4	42.1	29.8	36.7	44.5	57.6	46.4	54.2	49.1	62.3
Pb	14.3	19.8	12.9	14.8	9.6	17.1	7.2	36.1	41.3	55.6	31.8	63.5
Co	5	7	-	-	14.8	18.4	-	-	-	21.2	-	18.7
Cs	2.2	2	-	-	1.9	2.5	-	-	-	2.5	-	1.8
Hf	6.7	8.1	-	-	3.5	3.6	-	-	-	6.1	-	4.9
Ta	0.9	0.7	-	-	0.6	0.5	-	-	-	0.7	-	0.8
Th	9.6	10.1	-	-	4.5	4.3	-	-	-	8.1	-	6.7
U	2.1	1.8	-	-	2.1	1.3	-	-	-	2.4	-	1.5
Mo	7.2	6.8	-	-	3.5	4.3	-	-	-	4.1	-	4.2
Ag	0.4	0.3	-	-	0.4	0.3	-	-	-	0.3	-	0.4
La	9.8	11.1	-	-	17.3	16.7	-	-	-	20.3	-	22.2
Ce	27.2	30.2	-	-	38.6	36.7	-	-	-	42.7	-	45.3
Pr	3.48	3.79	-	-	4.85	4.69	-	-	-	5.39	-	5.68
Nd	14.7	15.9	-	-	20.8	19.6	-	-	-	22.4	-	23.4
Sm	2.76	2.89	-	-	4.57	4.06	-	-	-	4.82	-	4.75
Eu	0.61	0.58	-	-	1.34	1.08	-	-	-	1.22	-	1.27
Gd	2.33	2.46	-	-	3.71	3.42	-	-	-	4.21	-	4.17
Tb	0.4	0.42	-	-	0.58	0.53	-	-	-	0.66	-	0.63
Dy	2.41	2.53	-	-	3.53	3.13	-	-	-	3.97	-	3.53
Ho	0.52	0.54	-	-	0.73	0.66	-	-	-	0.81	-	0.72
Er	1.59	1.69	-	-	2.11	1.96	-	-	-	2.33	-	2.06
Tm	0.26	0.28	-	-	0.31	0.29	-	-	-	0.35	-	0.31
Yb	1.93	2.06	-	-	2.25	2.1	-	-	-	2.41	-	2.01
Lu	0.33	0.35	-	-	0.38	0.36	-	-	-	0.39	-	0.32
Eu/EU*	0.74	0.66	-	-	0.99	0.89	-	-	-	0.83	-	0.87
(La/Yb)n	3.43	3.64	-	-	5.20	5.38	-	-	-	5.70	-	7.47
((La/Sm)n	2.24	2.42	-	-	2.39	2.60	-	-	-	2.66	-	2.95
(Gd/Lu)n	0.87	0.86	-	-	1.20	1.16	-	-	-	1.32	-	1.60
(La/Lu)n	3.04	3.25	-	-	4.66	4.75	-	-	-	5.33	-	7.11
AI	1.13	1.10	0.65	0.80	0.70	0.81	0.80	0.79	0.74	0.63	0.73	0.64
ASI	0.83	0.86	0.89	0.95	1.06	0.94	0.88	1.11	0.97	1.12	1.06	1.08
Zr/Y	9.7	10.0	6.0	6.8	6.1	5.9	6.0	10.0	11.0	8.5	8.8	9.9

Highlights

- The hypabyssal and porphyritic Tarr albitites have a common petrogenetic origin
- Tarr albitites formed in a magmatic cupola accompanied by fenitization
- Dips of the contacts are consistent with the cupola apex above porphyritic phase
- Tarr albitites are late cumulates from fractionation of alkaline, tephritic magma

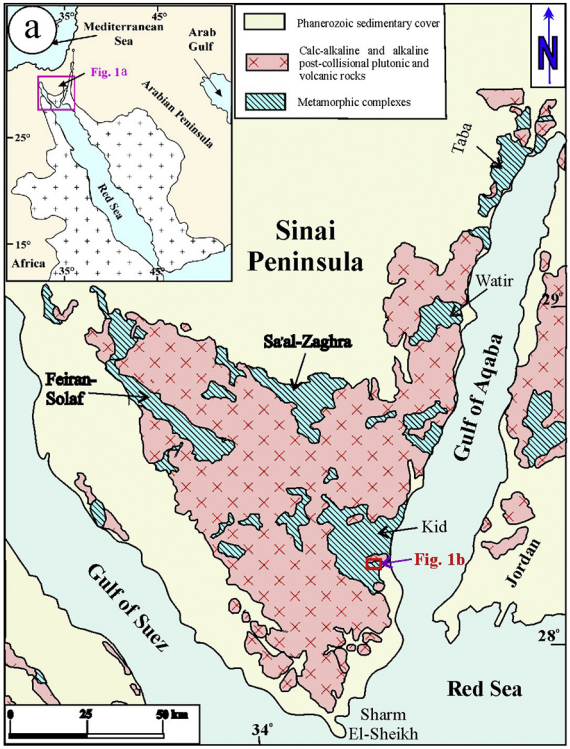
a
Mediterranean Sea
Arab Gulf
Fig. 1a
Arabian Peninsula
Red Sea
Africa
35°
45°
25°
15°
Phanerozoic sedimentary cover
Calc-alkaline and alkaline post-collisional plutonic and volcanic rocks
Metamorphic complexes
N
Taba
Sinai Peninsula
Watir
29°
Sa'al-Zaghra
Feiran-Solaf
Gulf of Aqaba
Kid
Fig. 1b
Jordan
Gulf of Suez
28°
Red Sea
Sharm El-Sheikh
34°
0
25
50 km

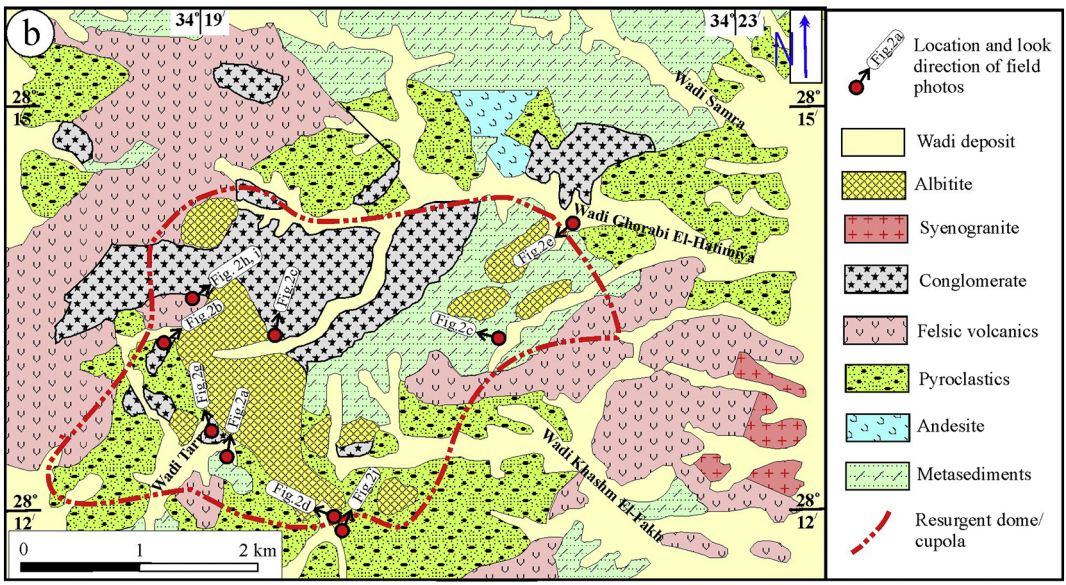
b
34° 19′
34° 23′
28° 15′
28° 12′
Wadi Samra
Wadi Ghorabi El-Hafimiya
Wadi Tarr
Wadi Khashm El-Fakh
Fig. 2a
Fig. 2b
Fig. 2c
Fig. 2d
Fig. 2e
Fig. 2f
Fig. 2g
Fig. 2h
0
1
2 km
Location and look direction of field photos
Wadi deposit
Albitite
Syenogranite
Conglomerate
Felsic volcanics
Pyroclastics
Andesite
Metasediments
Resurgent dome/ cupola

Figure 1

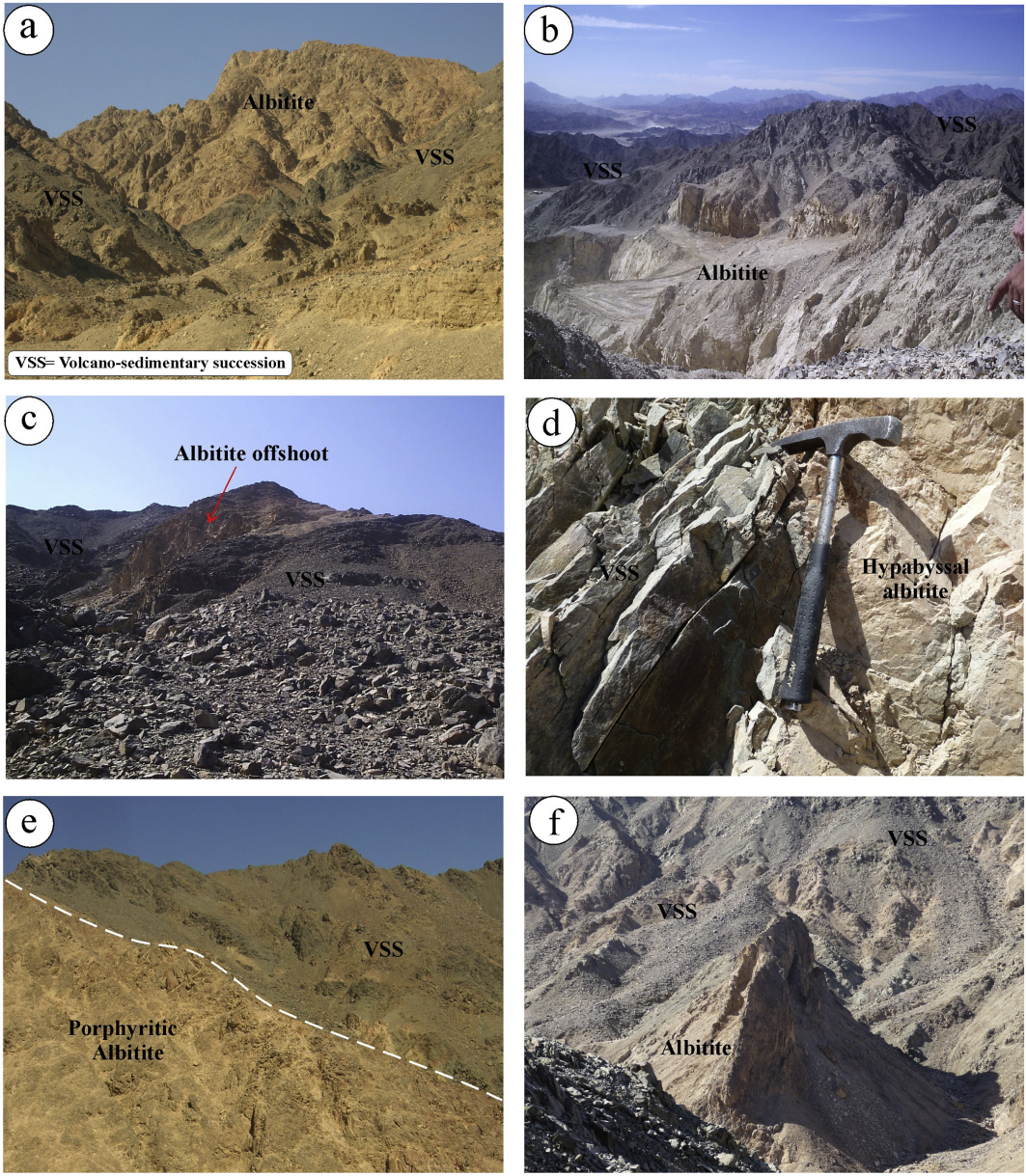
a
Albitite
VSS
VSS
VSS= Volcano-sedimentary succession
b
VSS
VSS
Albitite
c
Albitite offshoot
VSS
VSS
d
VSS
Hypabyssal albitite
e
VSS
Porphyritic Albitite
f
VSS
VSS
Albitite

Figure 2A


g
Hypabyssal albitite
Fenite zone
VSS
h
Albitite breccia
Volcanic breccia
i
j
Volcanic breccia
Intrusive carbonates

Figure 2B

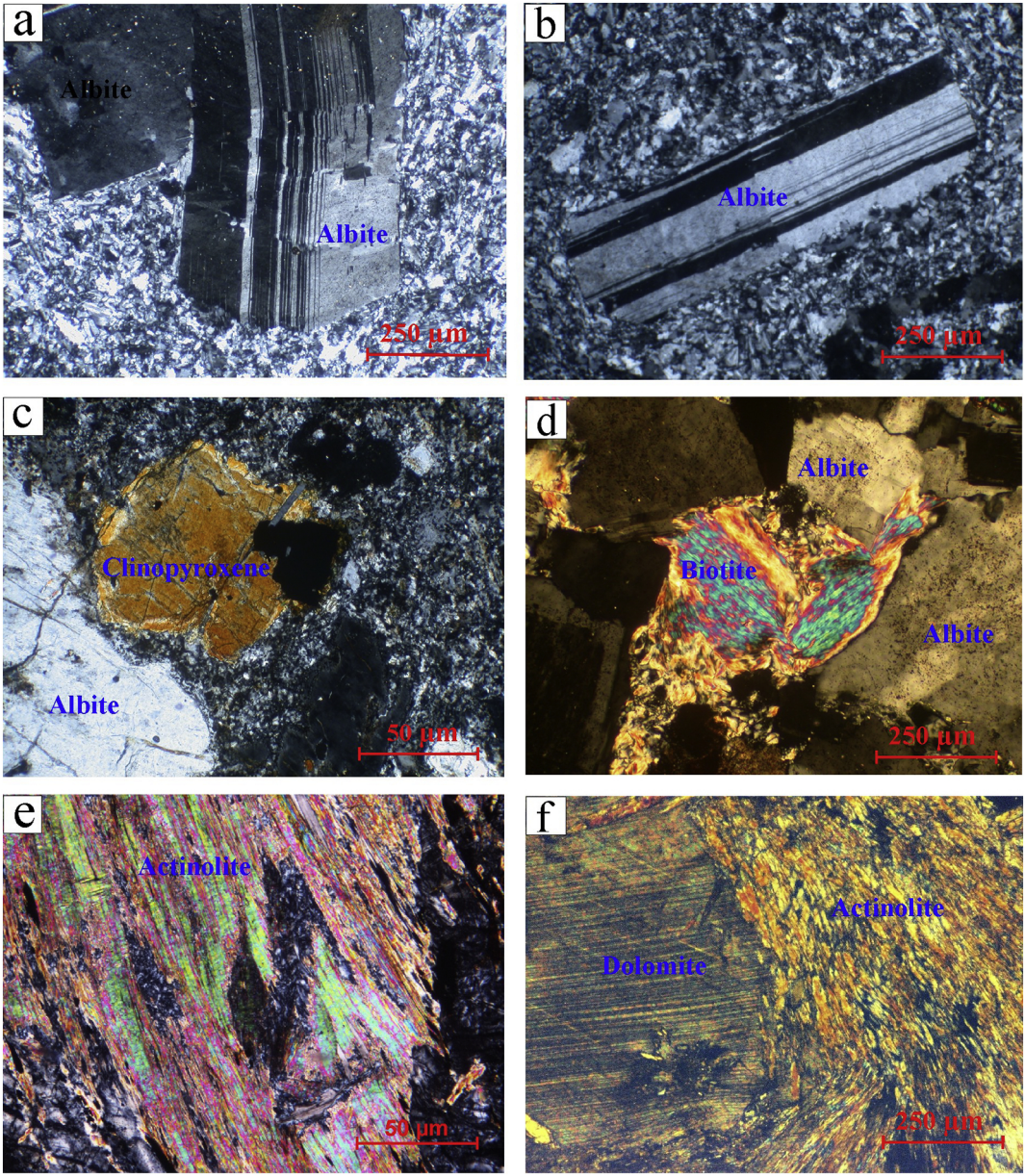
a
Albite
Albite
250 µm
b
Albite
250 µm
c
Clinopyroxene
Albite
50 µm
d
Albite
Biotite
Albite
250 µm
e
Actinolite
50 µm
f
Actinolite
Dolomite
250 µm

Figure 3A

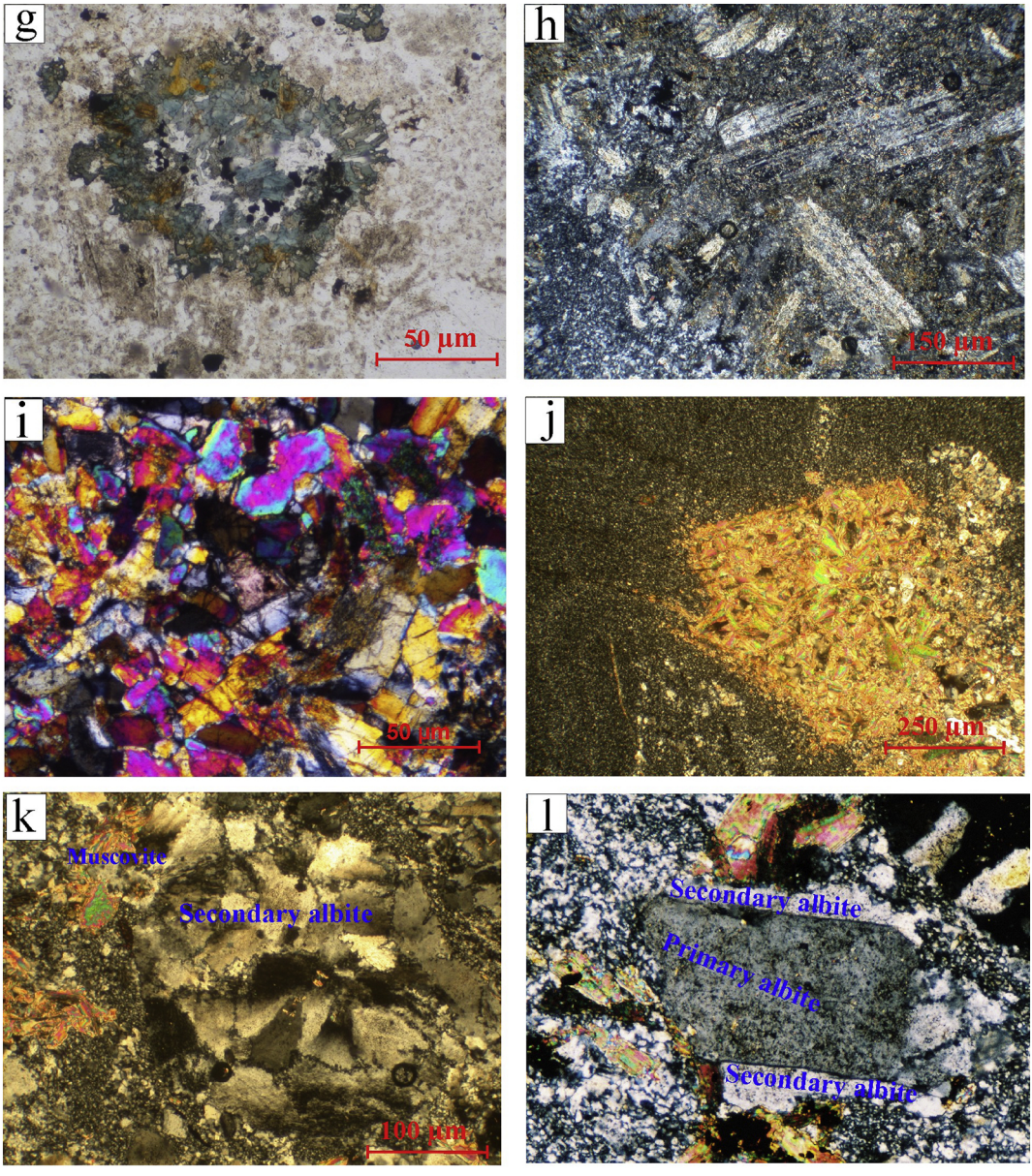
g
50 µm
h
150 µm
i
50 µm
j
250 µm
k
Muscovite
Secondary albite
100 µm
l
Secondary albite
Primary albite
Secondary albite

Figure 3B

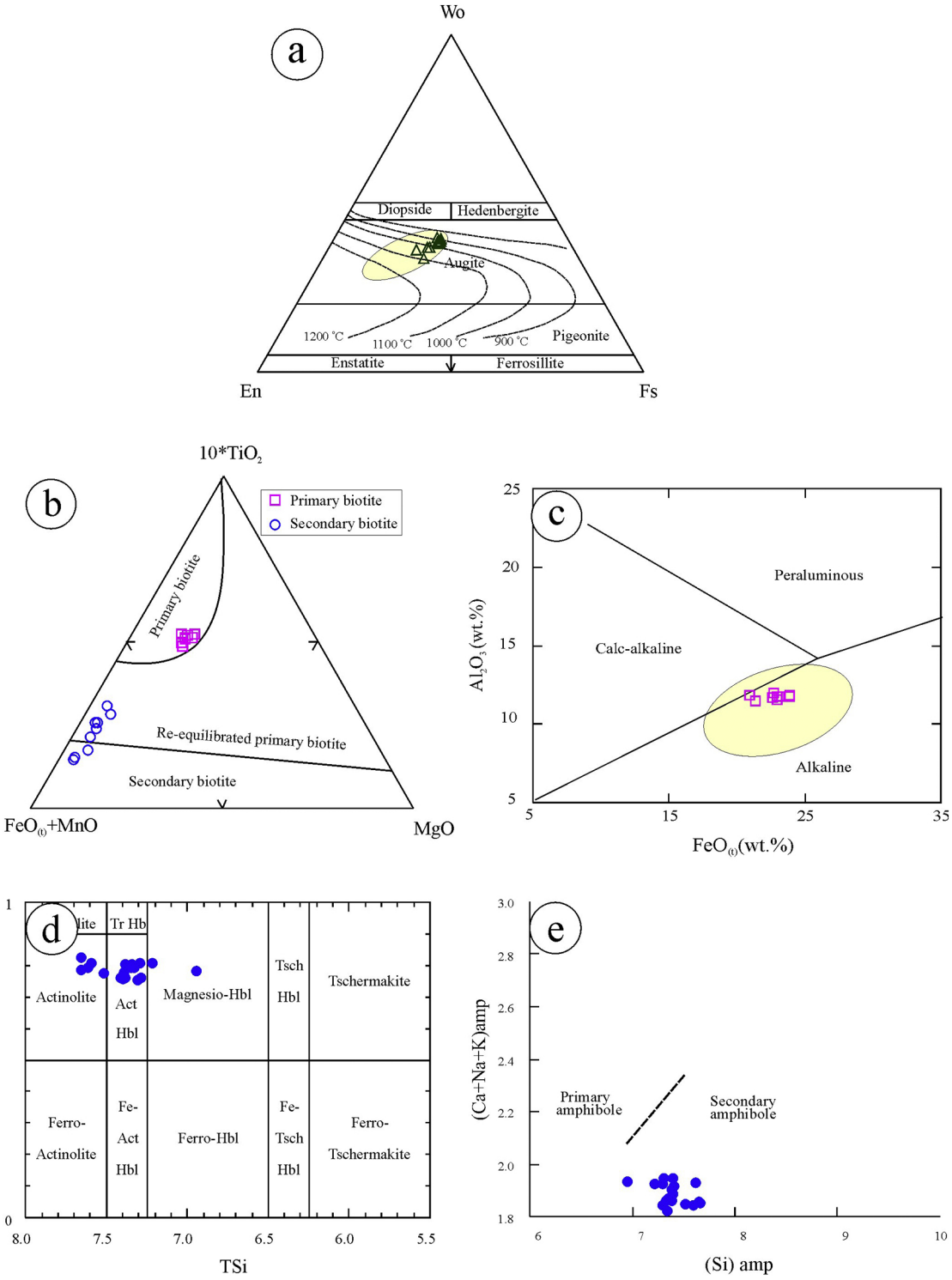
a
Wo
Diopside
Hedenbergite
Augite
1200 °C
1100 °C
1000 °C
900 °C
Pigeonite
Enstatite
Ferrosillite
En
Fs
b
10*TiO2
Primary biotite
Secondary biotite
Primary biotite
Re-equilibrated primary biotite
Secondary biotite
FeO(t)+MnO
MgO
c
Peraluminous
Calc-alkaline
Alkaline
Al2O3 (wt.%)
FeO(t)(wt.%)
d
Tr Hb
Actinolite
Act Hbl
Magnesio-Hbl
Tsch Hbl
Tschermakite
Ferro-Actinolite
Fe-Act Hbl
Ferro-Hbl
Fe-Tsch Hbl
Ferro-Tschermakite
Mg/(Mg+Fe2+)
TSi
e
Primary amphibole
Secondary amphibole
(Ca+Na+K)amp
(Si) amp

Figure 4

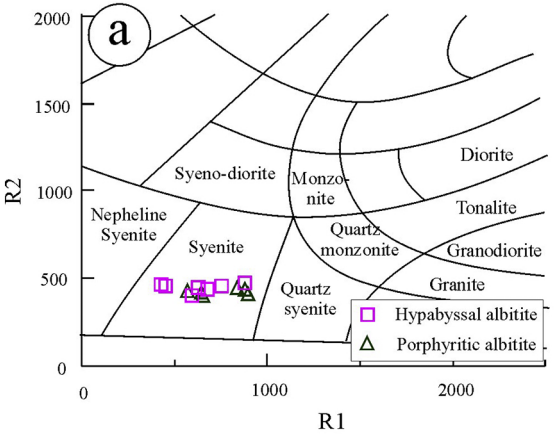
a
R2
R1
Syeno-diorite
Monzo-
nite
Diorite
Tonalite
Nepheline
Syenite
Syenite
Quartz
monzonite
Granodiorite
Granite
Quartz
syenite
Hypabyssal albitite
Porphyritic albitite

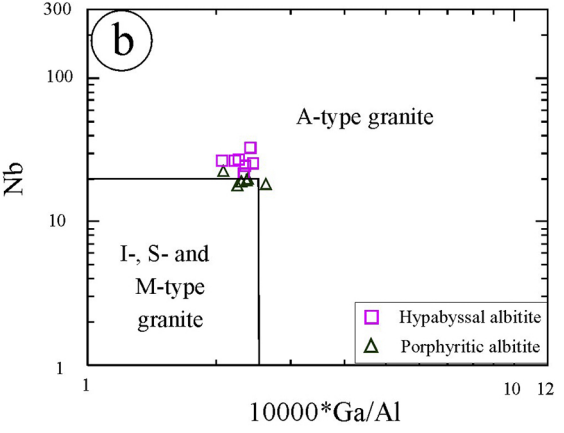
b
Nb
A-type granite
I-, S- and
M-type
granite
Hypabyssal albitite
Porphyritic albitite
10000*Ga/Al

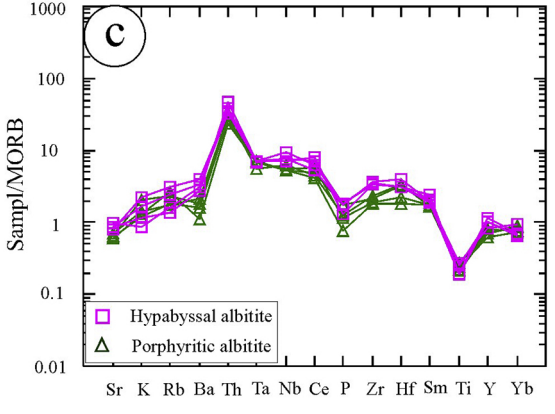
c
Sampl/MORB
Hypabyssal albitite
Porphyritic albitite
Sr K Rb Ba Th Ta Nb Ce P Zr Hf Sm Ti Y Yb

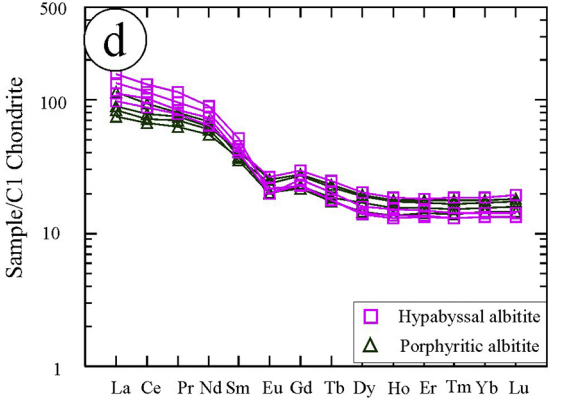
d
Sample/C1 Chondrite
Hypabyssal albitite
Porphyritic albitite
La Ce Pr Nd Sm Eu Gd Tb Dy Ho Er Tm Yb Lu

Figure 5

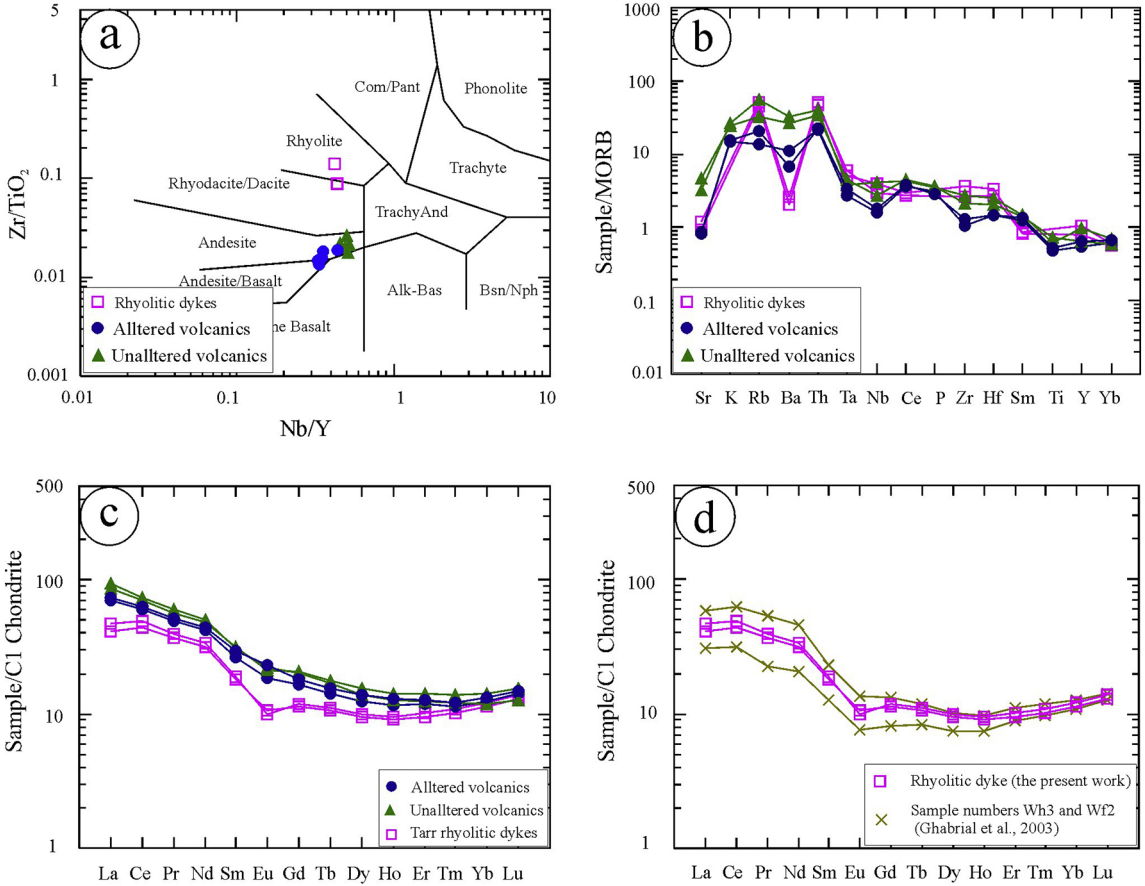
a
Com/Pant
Phonolite
Rhyolite
Trachyte
Rhyodacite/Dacite
TrachyAnd
Andesite
Andesite/Basalt
Alk-Bas
Bsn/Nph
Rhyolitic dykes
Alltered volcanics
Unalltered volcanics
Zr/TiO2
Nb/Y
b
Sample/MORB
Sr K Rb Ba Th Ta Nb Ce P Zr Hf Sm Ti Y Yb
c
Sample/C1 Chondrite
Alltered volcanics
Unalltered volcanics
Tarr rhyolitic dykes
La Ce Pr Nd Sm Eu Gd Tb Dy Ho Er Tm Yb Lu
d
Sample/C1 Chondrite
Rhyolitic dyke (the present work)
Sample numbers Wh3 and Wf2
(Ghabrial et al., 2003)
La Ce Pr Nd Sm Eu Gd Tb Dy Ho Er Tm Yb Lu

Figure 6

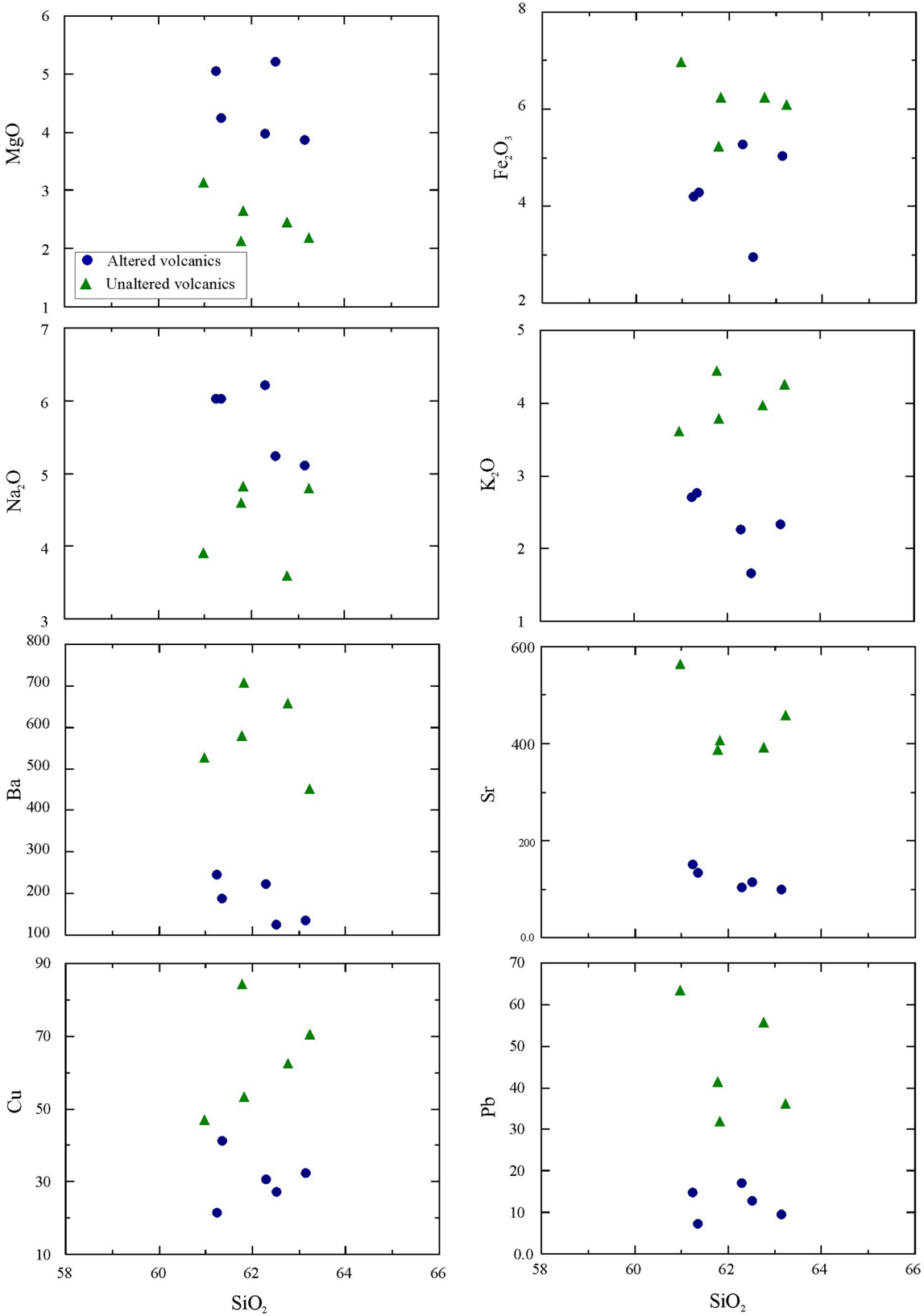
MgO
Altered volcanics
Unaltered volcanics
Fe_2O_3
Na_2O
K_2O
Ba
Sr
Cu
Pb
SiO_2
SiO_2

Figure 7

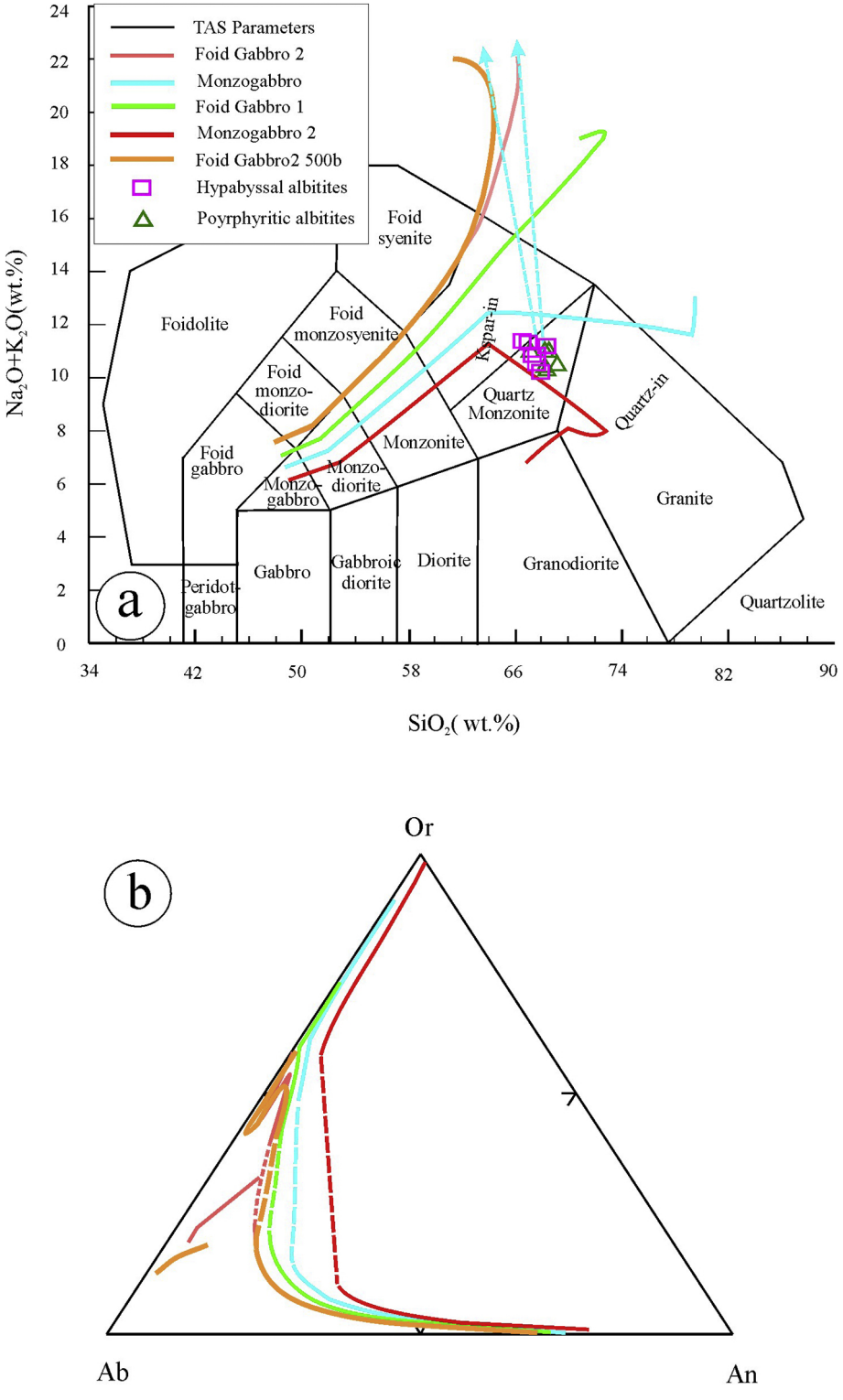
TAS Parameters
Foid Gabbro 2
Monzogabbro
Foid Gabbro 1
Monzogabbro 2
Foid Gabbro2 500b
Hypabyssal albitites
Poyrphyritic albitites
Foidolite
Foid syenite
Foid monzosyenite
Foid monzo-diorite
Foid gabbro
Monzo-gabbro
Monzo-diorite
Monzonite
Quartz Monzonite
Kspar-in
Quartz-in
Granite
Peridot-gabbro
Gabbro
Gabbroic diorite
Diorite
Granodiorite
Quartzolite
a
Na_2O+K_2O(wt.%)
SiO_2(wt.%)
b
Or
Ab
An

Figure 8

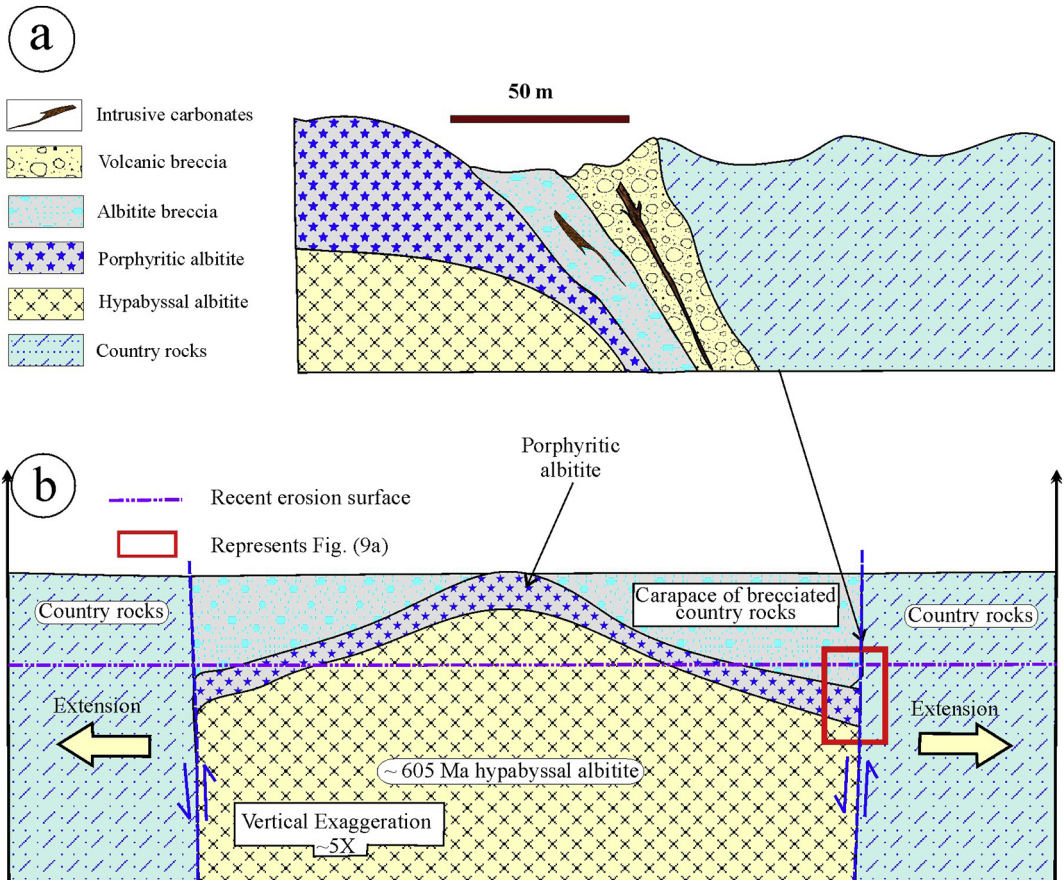
a
Intrusive carbonates
Volcanic breccia
Albitite breccia
Porphyritic albitite
Hypabyssal albitite
Country rocks
50 m
b
Recent erosion surface
Represents Fig. (9a)
Porphyritic albitite
Carapace of brecciated country rocks
Country rocks
Country rocks
Extension
Extension
~ 605 Ma hypabyssal albitite
Vertical Exaggeration ~5X

Figure 9